Nasa CR-65302

RADIANT HEATING SIMULATION

Second Phase Report

Prepared for

National Aeronautics and Space Administration
Manned Spacecraft Center
Houston, Texas

Contract NAS 9-3507

30 December 1964

[redacted]

Prepared by

T. K. Pugmire

Approved by

R. R. John

Research and Advanced Development Division
AVCO Corporation
Wilmington, Massachusetts

TABLE OF CONTENTS

I. SUMMARY

The overall objective of this study program is to define the requirements for simulation of the radiant heating attendant to atmospheric entry by manned spacecraft and assessment of techniques for achieving this simulation. Phase I of the study was to define the radiant heating inputs for manned missions. Phase II is an evaluation of existing radiant heater technology. A principal application of radiant heaters has been their use as energy sources for image furnaces. As this application is closely related to the present problem an attempt has been made to capitalize on the extensive technology and data available in the image furnace field. Descriptive information pertaining to several other non-image furnace sources is also presetned. No attempt has been made here to rate or select the preferred source from those described. This will be done during Phase III. Some additional information pertaining to the radiation heating environment is presented. This section also describes some problems encountered by researchers in this area as well as reports a new radiation heating prediction based on a new tool - a highly calibrated precision continuous arc source.

LIST OF SYMBOLS

The list below defines the principal notations used in the report.

E_t total equilibrium radiation per unit gas volume
$f(V_\infty)$ function of flight velocity
F_1 shock layer shape correction factor

F_2 thin film gage geometric view factor
P_1 initial pressure driven tube

$\dot{q}$ radiative heat transfer rate (energy flux per unit area per unit time).

R_N nose radius of hemispherical body

T transmissivity

V_s traveling normal shock velocity
V_∞ flight velocity

δ shock detachment distance

ρ_o reference density at STP conditions

ρ density (used as representing stagnation density)

Subscripts

g Gage property

∞ Flight, free-stream conditions

s Stagnation point gas property

II. INTRODUCTION

This is the Phase II, Report submitted under contract NAS 9-3507 and covers the period of 10 November through 30 December 1964.

A. Program Objective

Phase I - Definition of Radiant Heat Inputs for Manned Missions

1. This phase of the program shall include definition and characterization of the radiant heating environment associated with manned entry into planetary environments. Consideration shall be given to re-entry velocities from those characteristic of Apollo (35,000 to 45,000 ft/sec) to those characteristic of manned planned planetary missions (50,000 to 70,000 ft/sec and greater).

2. The Contractor shall investigate and report his findings of scaling and other simulation criteria necessary for predicting material behavior under radiant entry heating conditions. Particular emphasis shall be placed on investigating the necessary sample model size of the required spectral distribution of the energy from the radiant source, and of the necessity for programming the radiant heat input.

Phase II - Evaluation of Existing Radiant Heater Technology

1. A study shall be carried out on those radiant sources which might be utilized in entry simulation facilities. The following radiation sources shall be evaluated: a) Solid and gas discharge lamps; b) Electron beam heaters; c) Resistance or induction heaters; d) Solar furnace; e) Direct arc column heating.

2. The evaluation of the performance characteristics of the sources shall include: a) Maximum radiant flux attainable; b) Spatial and temporal uniformity of flux at test section; c) Spectral distribution of the radiant flux; d) Compatibility with convective heating sources; e) Operational characteristics; and f) Economics.

Phase III - Definition of Future Research and Development Requirements

1. On the basis of existing technology the state of the art of radiative and combined convective-radiative simulators shall be established.

2. Comparison shall be made between the state of the art of radiant heater technology and the future re-entry environment requirements. On the basis of this comparison specific recommendations for future development efforts shall be made if the existing technology is not adequate.

B. Program Organization

This program originates from the Structures and Mechanics Division of the NASA Manned Spacecraft Center. Mr. D. H. Greenshields, Thermo-Structures Branch is the Technical Representative for NASA MSC. The Project Director at AVCO/RAD is Dr. R. R. John. Mr. T. K. Pugmire

is the Project Engineer. Other participants in this phase of the study are Drs. T. Laszlo and R. Schlier and Messrs. M. Hermann, R. Liebermann, J. Morris, and F. Viles. R. Liebermann and J. Morris contributed in the area of environment definition. T. Laszlo provided data on a variety of radiation sources. R. Schlier, and F. Viles contributed information on several particular sources.

III. SOURCES

The radiation heating source consists primarily of the radiant energy source and in some instances an optical system for the concentration, focussing and modulation of the radiant energy.

1. Certainly the oldest and very likely the most spectacular source for radiant energy is the Sun.

Solar radiation is attractive because the source is freely available and the radiation arrives at the surface of the Earth with a sufficiently high intensity and in nearly parallel beams. The intensity of normal incidence solar radiation may be as high as 1.5 cal/cm^2-min at certain suitable sites. It is imperative to consider the normal incidence and not the total solar radiation, since only the well collimated fraction of the solar radiation can be concentrated in solar furnaces. This is the reason why dry, desert areas with high yearly solar irradiation values are not necessarily suitable sites for solar furnaces. The fine dust particles, which stay in the atmosphere above deserts for weeks after sand storms, disperse the solar radiation, causing a drop in the normal incidence value. In regions, where good ground cover exists, (vegetation during summer, snow during winter) atmospheric dispersion is small.

The apparent surface temperature of the Sun (approximately 6000°K) is very difficult to equal with any other radiation source, as is the approximately blackbody distribution of solar radiation. A very important feature of solar radiation is its stability when the sky is clear. It has been reported (reference 1) that on a clear day the intensity of solar radiation was stable within 5% for six hours. Figure 1 is an actual recording illustrating the constancy of the concentrated flux, (1).

The size of the image can be increased without decrease of the maximum flux by increasing the aperture of the concentrator. This is an expensive method, but image diameters as large as 5 inches are available in some large solar furnaces. With other sources the image cannot be increased beyond the size of the source without a decrease in flux.

The prime disadvantage of solar radiation other than the limitation on the maximum flux attainable is that it is not always available when needed. (This source was used by several laboratories during the mid 1950's as basic re-entry heating simulators.)

2. The Carbon Arc: Perhaps the most widely used radiation source is the carbon arc. The popularity has two reasons. First, the carbon arc is a familiar convenient laboratory source, ready for use whenever it is needed. Second, carbon arc sources are cheaply available from surplus searchlights and cinema projectors. In most cases these arcs are used without modifications in others changes in the mechanism are made to better suit the requirements. Generally the carbon arc is operated at a current of 150 amperes using a 16 mm anode. With special arrangements the current can be much higher, 300 amperes in the blown arc (3) and 3000 amperes when the entire mechanism is kept at 10 atm. pressure (4). In one controlled atmosphere carbon arc image furnace both the source and concentrator mirrors were enclosed in a nine foot diameter sphere (5). The sphere could be evacuated or pressurized up to 60 psi. The carbon arc was enclosed in a container which could be pressurized up to 210 psi. It was expected that with such a "concentrated" arc source such high flux can be radiated which at the receiver mirror focus would produce temperatures of 6000° to $10,000^{\circ}K$. No information on achieving this goal is available. Some systems operate at 2100 amperes without pressure (5). The following correlation between the arc current and flux at the focal area is given (7) for various electrodes in Table 1.

A high pressure arc, with tungsten-argon has been used in a closed system with liquid argon as the atmosphere sources (8). The arc has been operated up to a pressure of three atmospheres absolute, but could go higher. The maximum current for prolonged lengths of time (several minutes) was over 3000 amperes with 60 volts across the arc. The numerical value of the flux density at the second focus is not available, but it was very high.

The convenience of the carbon arc has to be balanced against it's two disadvantages. First, the flux stability is rather poor. The flux at the focal area of a commercial carbon arc image furnace was measured using a Gardon type radiometer. The result of this measurement is presented in Figure 2, (1). Similar measurements were performed on an improved (9) version of this furnace and the results are presented in Figure 3. These results show that there are two major flux instabilities in carbon arc image furnaces. The high frequency variations are caused by variations in electrode resistance, changes in electrode tip configuration, and variations in the solid particle content of the arc gap. The low frequency variations are caused mainly by changes in the electrode gap, unavoidable even with automatic feed mechanisms. The time/flux variations may be tolerated in certain experiments, when only the average flux is significant. In other cases, these variations may introduce very significant errors.

TABLE I. Operating and performance data for carbon arc double ellipical mirror image furnaces.

Lamp	Rotating carbon reflector lamp				Gretener super venlarc lamp
Mirror Diameter - inches	18				24
Mirror to crater distance - inches	6.5				7.5
Mirror to mirror distance - inches	70 3/16				96
Nominal magnification at intermediate focus	5.6X				6.5X
POSITIVE CARBON					
Type	High intensity	"Ultrex"	Modified "Ultrex"	Experimental	Experimental
Diameter - mm	11	11	11	10	12
NEGATIVE CARBON					
Type	Rod	Rod	Disk	Disk	Disk
Diameter - mm	8	8	270	270	270
Arc current - amperes	125	190	140	290	365
Arc voltage - dc volts	72-77	80-82	70	76	73
Arc power - kw	9.3	15.4	9.8	22.0	26.6
Positive consumption-inches/hour	25	45	50	160	140.0
Positive crater diameter - mm	10.6	10.9	9.3	9.6	11.6
Positive crater depth - mm	8.4	7.9	6.1	4.3	2.1
Center of crater brightness[b] C/mm^2	980	1680	1050	...	...
Center of disk brightness[b] C/mm^2	406	565	465	690	773
Brightness ratio-disk to crater	0.42	0.34	0.44	...	...
Diam. on image for ½ peak brightness - mm	8.0	8.5	9.0	11.0	13.8
Max irradiance on image - watts/mm^2	8.4	10.2	11.4	14.3	15.1
Diam. on image for ½ peak irradiance - mm	9.0	9.8	10.2	10.8	14.6
Blackbody temperature equivalent to maximum irradiance - °K	3510	3660	3770	4000	4050

a Brightness of a water-cooled surface of MgO at the image position-candles per mm^2.
b Brightness measured in direction axial to the source.

Second the continuous operating time of the carbon arc is limited by the length of the electrodes. At low current values one electrode lasts approximately 20 minutes, but at higher values only 5 minutes. Recently a new carbon arc has become available, which can operate 24 hours without interruptions (12). The carbons stored in metal cases are machined at both ends to male-female tapers respectively. The female tapered end of the new carbon is driven by a spring laden piston toward the male tapered end of the burning carbon. The passage of the joint into the arc is claimed to hardly affect the flux continuity. A second method to overcome this restriction is the use of two carbon arcs alternately in order to make extended runs possible. The mechanism for switching from one source to the other has to operate very fast in order to avoid a harmful temperature drop of the heated specimen. A third disadvantage is, that the carbon arc has to be placed at the first focus of the image. Consequently the two electrodes and the related equipment intercept a significant portion of the radiation emitted by the anode. In order to reduce this loss the use of an auxiliary mirror has been proposed (6). As illustrated in Figure 4, this reinforcing mirror replaces that portion of the image furnace paraboloid which is shaded by the cathode. Although the reinforcing mirror increases the shadow area, the increase in radiation intensity level is claimed to more than offset the increase in shading loss.

A different type of carbon arc, called "carbon vapor lamp" eliminates completely the shadow loss (11). This source uses three electrodes arranged radially and is supplied with three phase ac current (Figure 5). The arc operates in vacuum, thus reducing electrode consumption caused by oxidation. It is estimated that 8 inch long electrodes would last 8 hours, a significant value for continuous operation.

3. Electrical Resistors: A high refractory electrical resistor of suitable shape and dimensions can serve as a simple, convenient source. Flux stability is usually excellent, continuous operation for long periods is possible, and flux control is easily achieved at the source.

For low intensity a resistance heated tungsten filament projection lamp, G.E. type 2100 T24/8 can be used as a source of radiation. It is rated at 2100 watts when operated at 60 volts; under these conditions the life is 50 hours. As the operating voltage is raised, the expected life of the filament decreases, reaching 10 hours at about 68 volts. The filament consists of 8 parallel coils arranged in two planes. The filament coil assembly is nearly square ($\sim$1.2 cm on a side). As a result of use, a dark deposit develops on the inner surface of the glass envelope due

to evaporation of tungsten from the filament. This deposit may be removed when necessary by agitating a small quantity of abrasive powder sealed within the bulb. A 5 kw projection lamp when placed at the near focus of a 24 inch ellipsoidal mirror delivered at the far focus approximately 2 cal/cm^2 sec (12). Because of the large size of the filament array, the image is quite diffuse and non symmetrical.

Graphite resistors can be used for obtaining somewhat higher heat fluxes. These radiators are usually designed and fabricated by the experimenter to suit special requirements. When operated under inert gas protection they last long and deliver a very stable flux. A carbon resistor has been designed in such fashion that the use of an inert gas does not require a window (13). Thus no solid material of any kind is interposed between the source and the optics that may be required. The resistor mounting is designed so that the face of the resistor disk is the only hot part of the source that can radiate to the optics; the remainder of the resistor is totally enclosed by a water-cooled copper jacket. In addition to confining the effective source to a disk, this jacket makes possible the maintenance of an inert gas atmosphere around all the hot parts of the resistor by means of a flow of gas through the jacket. The arrangement is such that the gas enters through an opening in the mounting board behind the resistor and exits through a very narrow annular space between the disk and the jacket. The exit gas flow is at high velocity and is directed in such a manner that it converges to a point about 1 inch in front of the disk, thereby forming a protective cone of inert gas. A second gas channel is built into the jacket and is so designed that another slightly larger cone of gas is formed surrounding the first. The two directed gas flows result in a complete gas envelope around the face of the resistor without any physical confinement of the gas and hence without any significant absorption losses. At first helium was used for both the inner and outer cones, but convection currents led to incomplete cone formation. Since then argon has been used for the outer cone and helium for the inner cone with entirely satisfactory results. Apparently the heavier argon tends to contain the helium and convective disruption of the gas flow is prevented. A photograph of the resistor source with the jacket removed is presented in Figure 6. (The final vertical cut, which divides the base of the graphite into two sections, has not been made. Due to the fragility introduced by this cut, it normally is not made until the source is to be put into operation.) The success of this design may be judged from the fact that the resistor has been operated continuously for periods exceeding 4 hours at temperatures above 2,000°C with no visible signs of oxidation. This resistor can be used to sample temperatures up to 2,200°C.

Another carbon resistor operates in a dry argon atmosphere at 20 psig (14). The pressure is maintained by the use of a Pyrex hemisphere, the power leads are water-cooled (Figure 7). The resistor is operated at a maximum temperature of 2840°K, resulting in a flux of 15 cal/cm^{2}sec at the image. No provision is made for the removal of carbon vapor deposit which might be deposited at the inside wall of the hemisphere.

4. High Pressure Compact Arcs: These sources combine the brightness of carbon arcs with the maintenance-free and clean operation of incandescent lamps (15). They consist of a spherical or ellipsoid shape envelope, usually made of clear fused silica. Two diametrically opposed cylindrical extensions contain the metallic support and connecting rods for the two electrodes and the hermetic seals and carry the outer electrical contacts. The electrodes are made of solid tungsten and the bulbs are usually filled with xenon. (Figure 8) In operation the pressure within the lamp is between 6-30 atmospheres. Due to the high pressure the arc discharge fills only a small volume directly between the tips of the electrodes and thus forms a highly concentrated source. Operation and the performance data of various lamps are summarized in Table II (15). Lamps operated with ac give a more uniform brightness distribution than dc lamps. The stability of operation may be affected by the position of the lamp. Xenon dc arcs burn stable only when the cathode is at the bottom and the anode at the top. An image furnace using a 10 kw xenon arc as source has been completed recently (16). It is expected that the lamp will radiate approximately 5.5 kw.

5. Plasma Generator: Recently a concentrated effort has been applied tothe study of the plasma arc heater as a possible radiant energy source (17-20). The plasma arc heater is able to maintain an arc discharge with maximum temperature in excess of 20,000°K on a continuous time basis. The continuum radiation from such an arc column may be a few watts/cm to several tens of kilowatts/cm depending on the arc current, voltage gradient, pressure level and type of working fluid. This device has been utilized to provide a radiant and convective heating source for material specimens placed in the area vicinity of the arc column, (18). This type of source is also being developed for the single application of a radiating source, (17, 19, 20) In the latter case models are placed in the proximity of the column to be irradiated directly (Figure 9). Others are being developed with radiation collecting optics to increase the flux level at the target or model and to permit greater flexibility of model size, shape and placement. Such a device is shown in Figure 10.

TABLE II-A

MAIN DATA OF HIGH WATTAGE XENON, MERCURY, AND MERCURY-XENON COMPACT ARC LAMPS*

No.	Lamp Wattage watts	Type Designation	Gas/Vapor Filling	Max. Bulb Outer Diameter mm	Max. Over-all Length ins.	Arc Length in Operation mm	Internal Operating Pressure atm.	Lamp Operating Voltage volts	Lamp Operating Current amps.
1.	800 AC	SAH800C[a]	Hg	42	9 1/2	8.5	10	70	12
2.	900 DC	XB0900W[b]	Xenon	40	12 13/16	3.4		22	42
3.	1,000 DC	528B[c]	Hg-Xenon	45	7	6.5		65	16
4.	1,000 AC	SAH1,000A[a]	Hg	51	9 1/2	6.5	25	65	18
5.	1,000 AC	SAHX1,000A[a]	Hg-Xenon	51	9 1/2	6.5	30	65	18
6.	1,600 DC	XB01,600W[b]	Xenon	52	14 9/16	4.2		26	63
7.	2,000 DC	UXL2,000DK[d]	Xenon	53	14 3/16	6		28	70
8.	2,000 DC	XE2,000[e]	Xenon	54	14 13/16	3.5		22.3	90
9.	2,200 DC	491C[c]	Xenon	57	12 1/2	4	16	20-23	100
10.	2,500 DC	929B[c]	Hg-Xenon	64	12 1/2	4	18	45-55	50
11.	2,500 AC	SAH2,500A[a]	Hg	70	13	10	15	65	45
12.	2,500 AC	SAHX2,500A[a]	Hg-Xenon	70	13	10	20	65	45
13.	2,500 DC	SAHX2,500B[a]	Hg-Xenon	70	13	4.5	30	50	50
14.	2,500 DC	XB02,500W[b]	Xenon	57	16 7/8	6.2		30.1	83
15.	4,000 DC	UXL4,000DK[d]	Xenon		15 3/4	7		33	120
16.	5,000 DC[4]	932B[c]	Hg-Xenon	86	13 1/2	5	15	30-60	100
17.	5,000 DC	X35,000[e]	Xenon	89	19 1/2	7		34.5	145
18.	10,000 DC	XE10,000[f]	Xenon	92	27 1/2	8	10	40	250
19.	20,000 DC[4]	XE20,000[f]	Xenon	120	33 1/2	13.5	6	50	400

a. Westinghouse, USA
b. Oeram, West Germany
c. Hasovia, USA
d. Ushie Kegyo Katsha, Japan
e. General Electric, USA
f. Daro-Tem, USA

1. In vertical position 8 hours per start
2. 12 hours per start
3. Preliminary data
4. Experimental lamp

TABLE II-B

MAIN DATA OF HIGH WATTAGE XENON, MERCURY, AND MERCURY-XENON COMPACT ARC LAMPS*

No.	Lamp Wattage watts	Type Designation	Gas/Vapor Filling	Brightness Data - cd/mm^2			Initial Lumens	Initial Efficiency Lumens/Watt	Rated Life Hours
				Peak	Average for Arc Area of Width & Length mm				
1.	800 AC	SAH800C[a]	Hg	180			40,000	50	600
2.	900 DC	XB0900W[b]	Xenon		380	1.7 x 3.4	30,500	34	2,000
3.	1,000 DC	528B[c]	Hg-Xenon	970	230	2.5 x 6.5	52,000	52	1,000[2]
4.	1,000 AC	SAH1,000A[a]	Hg	475			50,000	50	300[1]
5.	1,000 AC	SAHX1,000A[a]	Hg-Xenon	475			50,000	50	400[1]
6.	1,500 DC	XB01,600W[b]	Xenon		430	2.1 x 4.2	56,000	35	2,000
7.	2,000 DC	UXL2,000DK[d]	Xenon		550	2 x 6	70,000	35	
8.	2,000 DC	XE2,000[e]	Xenon	4,100	820	3 x 3	85,000	42.5	500[3]
9.	2,200 DC	491C[c]	Xenon	3,300	440	2.3 x 4	75,000	34	1,000[2]
10.	2,500 DC	929B[c]	Hg-Xenon	2,050	540	2.5 x 4	120,000	48	1,000[2]
11.	2,500 AC	SAH2,500A[a]	Hg	325			125,000	50	400[1]
12.	2,500 AC	SAHX2,500A[a]	Hg-Xenon	325			125,000	50	200[1]
13.	2,500 DC	SAHX2,500B[a]	Hg-Xenon	2,050			120,000	48	400[1]
14.	2,500 DC	XB02,500W[b]	Xenon		450	3.1 x 6.2	100,000	40	1,500
15.	4,000 DC	UXL4,000DK[d]	Xenon		600	3 x 7	120,000	30	
16.	5,000 DC[4]	932B[c]	Hg-Xenon	2,250	780	3 x 5	230,000	46	
17.	5,000 DC	X35,000[e]	Xenon	5,900	870	5 x 5	275,000	55	500[3]
18.	10,000DC	XE10,000[f]	Xenon	9,500	1,250	5 x 5	480,000	48	500[3]
19.	20,000 DC[4]	XE20,000[f]	Xenon	7,500	1,700	5 x 5	1,000,000	50	

a. Westinghours, USA
b. Oeram, West Germany
c. Hasovia, USA
d. Ushie Kegyo Katsha, Japan
e. General Electric, USA
f. Daro-Tem, USA

1. In vertical position 8 hours per start
2. 12 hours per start
3. Preliminary data
4. Experimental lamp

Based on some experimental results with a plasma generator, 17, it was found that the radiation emitted by the arc column increased with increase in arc current (resulting in higher column temperatures of other factors are kept constant) and pressure level, but decreased with increase in mass flux rates mean voltage gradient and external magnetic field. These tests were made utilizing an argon arc column of 100-2000 amperes and pressure levels of 1-10 atmospheres. (Note: Some preliminary results indicate that in spite of the increase in radiation observed with higher pressure optimum operation may occur at pressure levels between 20 and 50 atmospheres.) Spectral distribution of several plasma generators operating with different working fluids were presented in the Phase I report.

Of the current plasma generators under development or currently being utilized as radiant sources the following four sources are somewhat representative.

a. A radiation source under development combines the effects of the vortex stabilized arc jet and the high pressure short arc. (20) A prototype of such a source is illustrated in figure 11. The arc chamber pressure is 17 atm. and the plasma temperature is approximately 7000^{O}K. When this source is operated under properly regulated power and gas flow, it produces a cylindrical arc plasma with a diameter approximately equal to that of the anode exhaust aperture. The cool vortex flow continually replaces the gas surrounding the arc, thus greatly reducing the red and infrared radiation as compared to other enclosed arcs. Also the vortex fixes the arc plasma diameter and precisely locates the arc column. The total radiant output of a 10 mm x 3 mm arc plasma is reportedly 7.68 kw, with an input of 24.8 kw when operated with argon.

b. A somehwat different approach is utilized in the device shown schematically in Figure 12, (19). In this source the radiating plasma is isolated away from the sustaining portion of the arc heater (gas inlets, electrodes, insulators) so that there is little obstruction to theradiation except on one side. The reported operating conditions are input power 25 KW (units capable of operation at power levels up to 50 KW are under development), 0-300 PSIG chamber pressure and a 6 mm diameter luminous sphere with a radiant efficiency of 35% when operated with argon at 25 KW.

c. A very useful device that has been used as a combined radiative and convective heating source has been referred to as a modified tandem Gerdien arc (18). In this source the test gas, air or other gases of interest, is heated in an arc column which is partially constricted by vortex flow and by mechanical orifices, Figure 13 (18). The test model is positioned in the close

proximity of the arc column which provides the radiant energy. Radiant energy transfer can be changed by varying the distance between this model and the column. Previous column temperature measurements made on an arc of this type indicated peak temperatures between 16,200-18,000^{o}K (21).

The temperature profile of the column has not been reported. Slightly less than 800 BTU/ft^2-sec radiative heat transfer from air was measured by a radiation cavity gage at a distance of approximately 1 cm from the column boundary, with an input of 250 KW and one atmosphere chamber pressure. A unit is currently under development which will allow operation at pressures up to 5 atmospheres and permit location of the model effect on model performance resulting from the non-uniformity of the source as most models tested have been char formers which to tend to nulify such non-uniformities (22).

d. The fourth source of this type that is of interest is similar to that described in section a (20). The principal differences are in the operating condition, i.e. higher power levels and chamber pressures, and in the associated optics. This device, shown in Figure 10, has produced a radiating efficiency of about 35% when operated at 100 KW, 25 atmospheres and 800 amps. It is expected that this source will produce a usable directed radiation beam which has a total efficiency of over 5% with respect to the total input power. Four of these sources are being installed in conjunction with a high enthalpy 2½ megawatt arc heater for a combined variable radiative and convective heating facility, Figure 14.

6. Electron Beam Radiation Sources: Electron beams, consisting of a directed stream of voltage accelerated electrons in a vacuum of pressure less than 10^{-3} or 10^{-4} torr, may be considered as radiation sources, both directly, as in the case of the electron microscopy, or indirectly as a well defined heat source for a primary thermal radiation emitter. All electron beam equipment has certain common elements, however there is a great divergence in size, beam resolution, beam control and power according to the design application. Common functionally described parts for all systems are:

a. Electron gun which contains an emitter, and some directive provisions. A negative voltage control grid is used in precisely regulated equipment.

b. High voltage power supply to accelerate the electrons.

c. A target area of conductive material,

d. A sealed chamber with an insulated support for the gun target accesses, a high capacity vacuum pumping equipment capable of 10^{-3} to 10^{-6} torr vacuum, and X-ray shielding (23).

All beam operations are performed at the low pressure, except some recent in atmosphere welders, which pass the beam through a series of holes that are pumped to prevent gas from reaching the gun.

Reliable and precise equipment prices start at $70,000 and up depending upon refinements in the beam controls and accuracy of power measurements. The operating characteristics of this equipment are a capability to focus up to 6 kilowatts into a spot which is 0.003 inches diameter. At lower power smaller spots may be obtained. For a lower heat flux, a defocussed spot may be used at the sacrifice of spatial distribution uniformity, since the power density is usually described as Guassian through the spot. A spot diameter is usually defined as the diameter containing one half the beam power. The voltage is variable up to 150,000 volts and the amperage up to 40 milliamps in a 6 KW machine. The focussed beam has a long focal length (up to 15 inches) and auxiliary deflection circuits and current modulation circuits can produce uniform power density patterns, similar to a television screen raster up to 5 inches square. The spatial uniformity is then dependent upon line overlap and lines per inch. Complete feedback voltage and current regulation can be provided which would result in a temporal stable beam. On a sweeped raster, temporal energy distribution is dependent on the number of lines and the x-y coordinate sweeping frequencies. Instrumentation to measure beam current and voltage can provide control of power to better than 1% and modulation can modify power distribution to compensate for heat loss at edges of thermally conducting targets.

The direct application of electron beams to simulate infrared, visible, or gamma radiation sources for purposes of materials testing is not advised. For example a beam accelerated by 15,000 volts would provide optical properties of resolution comparable with gamma radiation of 0.1 $\AA$, the radiation intensity would be quite high in comparison with standard optical sources.

Therefore, the application of electron beams to radiation simulating devices is restricted to the application of a heat source for a hot body radiator. For relatively small targets of several square inches, up to 500 BTU/ft^{2}sec could be applied with well controlled distribution to assure spatial uniformity of temperature of the primary radiation source. The radiation from this source would be temporarily stable after initial heating,

but at least one half of the power would be directed to the reverse side of the target and lost unless a special collector system could be used to collect and redirect some of the reverse transferred energy. The spectral distribution of the electron beam heated primary emitter is that of a black body at the same temperature as modified by temperature dependent spectral emittance coefficients of the target material and any additional windows or optics as may be required.

7. Lasers as Radiation Sources: The laser, or optical maser, provides a coherent light output at power levels ranging from watts for the recently developed continuous wave gas lasers to gigawatts for short-pulsed (a few nanoseconds) solid-state optically pumped ruby lasers. Because the light output is coherent, it can be focussed to a diameter approximating the wavelength of light, so that flux levels as high as 10^{17} watts/cm^2 are attainable in principle.

Lasers can therefore provide almost any conceivable radiant flux. Their usefulness as a simulation source, however, is severely limited by the fact that the total output energy, and the duration of the output pulse, are both circumscribed. In addition, the light output is monochromatic.

Since other light sources (arc discharges, for example) can provide radiant fluxes as high as 10^4 watts/cm^2, there appears to be no purpose in the use of lasers for simulation purposes at this and lower flux levels. At higher levels, lasers can serve a useful purpose, but not as a simulation radiation source. This is because the pulse duration of high energy lasers is limited, at the present time, to a few milliseconds. For example, one can obtain, with present ruby laser devices, a total energy output of over 1000 joules, with a pulse duration of about 2 milliseconds. This would provide a radiant flux of 10^5 watts/cm^2 on an area of 5 cm^2, and, by reducing the area, a flux of 5×10^7 watts/cm^2 on 1 sq. mm.

The short duration of the pulse makes it unusable for materials testing as there is insufficient time for the material under investigation to attain quasi-steady-state conditions, except at very high flux levels.

The one potential use of lasers appears to be as a means of investigating the basic phenomena that occur at high radiant flux levels. This is particularly the case at flux levels that are higher than those presently attainable with flash tubes.

The laser presents other advantages, for fundamental investigations, in that its output is monochromatic, the output energy and flux are readily controlled, and it is a relatively clean source of radiant energy. Associated electromagnetic noise can be almost completely eliminated, so that measurement techniques requiring sensitive electronic detection are feasible.

IV. RADIATION HEATING DEFINITION

1. Comparison Studies of Experimental Radiation Data

Comparison studies have been made with radiation data obtained experimentally from shock heated gas. Graphical representation of these data are shown in figures 15 through 18 for air as a function of flight velocity.

Figures 15 through 18 present shock tube total stagnation-point-region, equilibrium-radiation data measured by four independent investigators (Ref. 24, 25, 26 and 27) who utilized different measurement techniques. For convenience of comparison the stagnation-point-regions volumetric-radiation was normalized using the relationship that

$$E_t \propto \left(\frac{\rho}{\rho_o}\right)^{1.7} \cdot f(V_\infty) \qquad (1)$$

Where the above equation was suggested by references 27 and 28. Figure 19 is a composite comparison of the equilibrium data presented in figures 15 through 18. As will be subsequently pointed out in the following section, erroneous results were found in the data of references 25 and 26, however, Figures 15 through 19 present these data in the corrected form.

2. Reduction of Shock Tube Data

In the reduction of shock tube data, heating rates of test surfaces, due to radiation from shock heated gas, are distinguished from heating rates due to convective heat transfer by several means. For example, when the test probes have large nose radii, the radiative contribution at the stagnation point region is large enough to become the dominant mode of heat transfer and direct measurments of radiation can be made utilizing thin film resistant thermometers or thick film calorimeter gages (see reference 24). Another method is by means of locating on the test probe a transparent window through which incident radiant energy from the shock heated gas cap is transmitted and collected by a thin film radiative heat transfer gage. This latter technique was utilized by both references 25 and 26, however, reference 25 used a hemespherical faced probe while reference 26 used a blunt faced probe. Finally as was performed by reference 27, measurements utilizing photomultiplier tubes may be made of the total radiation from shock layers of gun-launched models flying in still air or moving upstream in the test section of a shock tunnel.

Once the above data is obtained, its reduction into terms of total radiation emitted from the stagnation point region requires further analysis. The first and probably most important analysis is determining whether the radiant energy so collected and measured is due primarily to non-equilibrium conditions, equilibrium conditions, or a combination of both in the shock heated gas cap. When equilibrium conditions are known to prevail and direct radiation measurements can be made, the total equilibrium radiation, E_t, at the stagnation point region, may be calculated from the following semi-emperical equation.

$$E_t = 2\,\dot{q}_{rad,\,stag.\,Pt.} / \delta F_1 \qquad (2)$$

where $\dot{q}_{rad,\,stag.\,Pt.}$ is the radiative power flux measured at the stagnation point region of the probe, δ is the shock detachment distance and F_1 is a correction factor taking into account the shape of the shock front and thermodynamic variations therein. It was reported by Nerem[25] who in turn referenced Wick[29] that F_1 is approximately 0.84 and the ratio δ/R_N is approximately 0.045 for a probe of hemispherical nose radius R_N in the flight velocity range of 20 x 10^3 to 60 x 10^3 ft/sec and at simulated altitudes of 100×10^3 ft to 240×10^3 ft. In addition, It was reported by Page[27] that the ratio δ/R_N could also be closely approximated in the above flight range by the relationship:

$$\delta/R_N \simeq \frac{3}{4} \cdot \frac{\rho_\infty}{\rho} \qquad (3)$$

For test probes utilizing transparent windows the total equilibrium radiation, E_t, may be calculated from a semi-emperical relation having the form:

$$E_t = 2\,\dot{q}_{rad,\,gage} / \delta F_1 F_2 (T) \alpha_g \qquad (4)$$

where $\dot{q}_{rad,\,gage}$ is the radiative power flux seen by the collector gage, F_2 being its view factor and α_g its absorptivity. T is the transmission coefficient of the transparent window. F_1 and δ are as discribed above.

a. Reduction of Flagg's Data[24]

Flagg's Data[24] was obtained in the form of figure 20. It was necessary to correct his ratio $\dot{q}/R_N$ into total equilibrium radiation, E_t, emitted from the stagnation point region. This was accomplished utilizing equation (2). The choice of F_1 and δ values were those suggested by Wick[29], since it was determined that Flagg's data simulated flight velocities and altitudes were Nerem[25] stated F_1 = 0.84 and δ/R_N = 0.045. Flagg's stagnation density ratios ρ/ρ_∞ and simulated flight velocities were determined using shock tube gas dynamic charts.[30] By use of reference [30] all flight conditions for Flagg's data were known. Therefore it was of interest to compare Wick's[29] approximation of the ratio δ/R_N against Page's[27] (equation 3). Page's approximation[27] yields values of δ/R_N for Flagg's data from δ/R_N = 0.0625 to 0.0595 (a discrepancy of approximately 30%). Hence the shock tube data so plotted in figure 15 is questionable.

b. Reduction of Nerem's Data[25]

Nerem[25] published all of his data in a tabulated form giving initial shock tube driven pressures, P_1, shock velocities, V_s,

simulated flight velocity, V_∞ , stagnation density ratios, ρ/ρ_o, ect. Thus no reduction of his data was necessary. However, by examining Nerem's data reduction procedure, it was established that he used shock tube gas dynamic charts published by Zimer (1960)[31], and since Nerem's tabulated data gave adequate parameters, a comparison was made against the shock tube gas dynamic charts published by Laird J. D. and K. Heron[30] (1964). Several discrepancies were found. Differences up to 25% were found in stagnation density ratios (Nerem's values being high). Nerem's calculated results indicating a constant stagnation density ratio ρ/ρ_o for a constant initial pressure P_1 was also in disagreement with reference [30]. And it was established that Nerem overestimated his flight velocities, V_∞ , by 3%. Although these errors are comparable to shock tube experimental scatter, the data so presented in figures 15 through 19 are very sensitive to density and flight velocity, and the magnification of the already present experimental scatter makes direct comparisons difficult. Nerem's density values were corrected using reference 30 and this data is shown in figures 16 and 19.

Another distrubing feature, brought out by the above discrepencies is the shock detachment distances, δ, calculated by Nerem in his data reduction (see equations (3) and (4)). The means used by Nerem to determine his shock detacment distance, δ , is not known at this time. However, if it were as of equation (3) then his detachment distances are questionable (upward to 25%) also. Therefore, the reliability of Nerem's data as shown in figure 16 is questionable.**

c. Reduction of Hoshizaki data[26]

Unlike Nerem[25], Hoshizaki[26] did not tabulate his results. His data was presented in his report in the form of figure 21. As seen in figure 21, Hoshizaki data was calculated to have a stagnation density ratio of .193 for an initial pressure P_1 = 1.16 mm H_g.*

An investigation of Hoshizaki's data was made utilizing the shock tube gas dynamic charts of reference[30]. A discrepancy of 25% in stagnation density ratio was found (Hoshizaki's value being high.) Hoshizaki did not reference use of any gas dynamic charts, however it was learned[32] that Hoskizaki used Ziemer's[31] charts and, after publication, was aware that Ziemer's charts were outdated. No further investigation was made into the reduction procedures of Hoshizaki. As presented in figures 17 and 19, his data has been corrected using reference 30.

---

*It is of interest to note that Nerem[25] reported this same data in his report as ρ/ρ_o = .16 and P_1 = 1.0 mm H_g.

** Prior to publication of this report a telephone conversation with R. M Nerem revealed that Nerem[25] was aware, after his publication that Ziemer charts[31] were outdated. However Nerem stated that his shock detachment distances were obtained experimentaly and were not dependent on the density relation given in equation (3).

d. Reduction of Pages Data[27]

Page W. A, et al[27] tabulated his experimental results in a form where no reduction of his data was necessary. His equilibrium radiation data is plotted in figures 18 and 19.

One disturbing feature of Pages et al Report is that he did cite Ziemer's gas dynamic charts.** This raises the question as to the reliability of his calculated density ratios.* As was noticed in the data of Neren[25] and Hoshizaki[26], Ziemer's charts tend to over estimate these ratios for a given set of initial shock tube conditions with the descrepancies being more pronounced at the higher density values. Therefore, it must be concluded that Page's data so plotted in figures 18 and 19 are also questionable in excess of their exibited experimental scatter.

3. Conclusions and General Remarks

As pointed out in the preceding sections, published radiation data obtained via shock heated gas experiments is of question - greatly influenced by the reliability of gas dymanic charts and theoretical models used in describing the gas cap. However it must be argued that the above described means for obtaining radiative data are representative of each other within approximately a factor of two (see figure 19).

* It should be noted here that until recent time gas dynamic charts by Feldman[33] have been widely used in shock tube work. Feldman's charts were recently expanded in terms of flight conditions and are represented by reference [30]. It is generally accepted that reference 30 represents the present state of the art in shock tube gas dynamic charts.

** Page also cited Feldman gas dynamic charts[33], but it is not clear as to which charts he actually used.

REFERENCES

1. Foex, M., "Concerning Several Devices for the Utilization of Imaging Furnaces", Proceedings Int. Conf. Image Furnace Techniques, Cambridge, Mass., Plenum Press, Inc., New York, N. Y. (1964).

2. Laszlo, T. S., Unpublished Data.

3. Glaser, P. E., "Imaging Furnace Developments for High Temperature Research", J. Electrochem. Soc. 107, No. 3, (1960).

4. Cook, J. C., "A 400 KW Pressurized Arc Imaging Furnace", Proceedings Int. Conf. Image Furnace Techniques, Cambridge, Mass., Plenum Press, Inc., New York, N. Y., (1964).

5. Horning, D. O. and Parker, E. R., "Arc Image Furnace" AFOSR TR-59-88, May (1959).

6. Denney, K. L., McDonnel Aircraft Corporation, St. Louis, Mo., Private Communication to T. S. Laszlo.

7. Null, M. R. and Lozier, W. W., "Carbon Arc Image Furnaces", Rev. Sci. Inst., Vol. 29, No. 2, 163-70, February (1958).

8. Hazlett, T., University of California, Livermore, California, Private Communication to T. S. Laszlo.

9. Farmer, R. W., "An Arc-Imaging Furnace for Materials Research", ASD-TDR-63-312, May (1962).

10. Latil, J. P., "Automatic Recarboning of Carbon-Arc Lamps", Jour. of the SMPTE Vol. 66, June (1957).

11. Ploetz, G. P., Cox, H. F., and Larson, L. C., "The Carbon Vapor Lamp: A Thermal Radiation Source for Imaging Furnaces", Proceedings Int. Conf. Image Furnace Techniques, Cambridge, Mass. Plenum Press. Inc., New York, N. Y., (1964).

12. Cotton, E. S. Quartermaster Research & Engineering Center, Natick, Mass., Private Communication to T. S. Laszlo.

13. Maust, E. E. and Warnke, W. E., "The Performance and Operating Characteristics of an Image Furnace Having 60-inch Paraboloidal Mirrors", Bureau of Mines Report of Investigations 5946, (1962).

14. Richardson, D. L., "A Thermal Radiation Heat Source and Imaging System for Biomedical Research", Proceedings Int. Conf. Image Furnace Techniques, Cambridge, Mass., Plenum Press, Inc., New York, N. Y., (1964).

REFERENCES
(Cont'd)

15. Thouret, W. E. and Strauss, H. S., "High Wattage Xenon and Mercury Vapor Compact Arc Lamps as Radiation Sources for Imaging Furnaces", Conference on Imaging Techniques, Cambridge, Mass., 4-5 October 1962.

16. May, C. E., NASA Lewis Research Center, Cleveland, Ohio, Private Communication to T. S. Laszlo (1962).

17. Hermann, M., and Liebermann, R., "An Investigation of Radiation Emitted for a High Temperature Arc Column and Its Potential as a Source for High Radiant Heat Flux Simulators," R530-63-82, AVCO Research and Advanced Development Division, Technical Symposium, Denver, Colorado, March, 1964.

18. Diaconis, N. S., Weber, H. E. and Warren, W. R., Jr., "Techniques for Severe Radiative and Convective Heating Environments for Materials Evaluation," Third Hypervelocity Techniques Symposium, Denver, Colorado, March, 1964.

19. "Vitro High Energy Plasma Source", Vitro Corporation of America.

20. "Vortex Stabilized Radiation Source", Plasmadyne Corporation, Santa Ana, California, PRE-106.

21. McGinn, J. H., "A New Type Arc For Producing High Temperature, High Purity Plasma Jets; Proc. 5th Int. Conf. on Ionization Phen. in Gases, Munich, 1961, North-Holland Pub. Co., Amsterdam.

22. Lundell, John H., Nasa Ames Research Center, Moffett Field, Calif., Pivate Communication to T. K. Pugmire.

23. Bakish, R., (ed.). Introduction to Electron Beam Technology, John Wiley & Sons, 1962, Congress No. 62-17262.

24. Flagg, R. F. "Stagnation-Point Radiative Heat-Transfer Measurements at Supersatellite Velocities" Avco Research and Advanced Development Division Wilmington, Mass. RAD-TM-63-77, Dec., 1963.

25. Nerem, R. M. and G. H. Stickford, "Shock Layer Radiation During the Hypervelocity Reentry", AIAA paper, Entry Technology Conference October 12-14, 1964; Nerem, R. M., "Stagnation Point Heat Transfer in High Enthalpy Gas Flows", Part I and Part II, Ohio State University Aerodynamic Laboratory Final Report, prepared under contract AF 33(657)-10110, Research and Technology Division, Air Force Systems Command, Wright-Patterson Air Force Base, Dayton, Ohio, FDL-TDR-64-41 March, 1964.

26. Hoshizaki, H., "Equilibrium Total Radiation Measurements in Air at Superorbital Entry Velocities", Lockheed Missiles and Space Co., Rept. No. 6-90-63-97, October, 1963.

27. Page, W. A. and J. O. Arnold, "Shock Layer Radiation of Blunt Bodies Traveling at Reentry Velocities", NASA TR-R-193 April, 1964.

28. Allen, R. A., P. H. Rose, and J. C. Camm "Non-Equilibrium and Equilibrium Radiation at Super-Satellite Reentry Velocities", IAS Paper No. 63-77, Presented at the IAS 31st Meeting, N. Y., N. Y. Jan., 1963.

29. Wick, B. H., "Radiative Heating of Vehicles Entering the Earth's Atmosphere", Presented to the AGARD Fluid Mechanics Panel, Brussels Belgium, April 3-6, 1962 (NASA Document No. N62-12453).

30. Laird, J. D., and K. Heron, "Shock Tube Gas Dynamic Charts" Part I "Equilibrium Argon-Free Air from 3,000 to 40,000°K", Avco Research and Advanced Development Division, TM 64-12, April 10, 1964.

31. Ziemer, R. W., "Extended Hypervelocity Gas Dynamic Charts for Equilibrium Air", Space Technology Laboratories, Inc., Report STL-TR-60-0000-09093, April 14, 1960.

32. Personal communication with Dr. K. Heron[30] who had previous communication with Hoshizaki[26].

33. Feldman, S., "Hypersonic Gas Dynamic Charts for Equilibrium Air", Avco Everett R. R. 40, 1957.

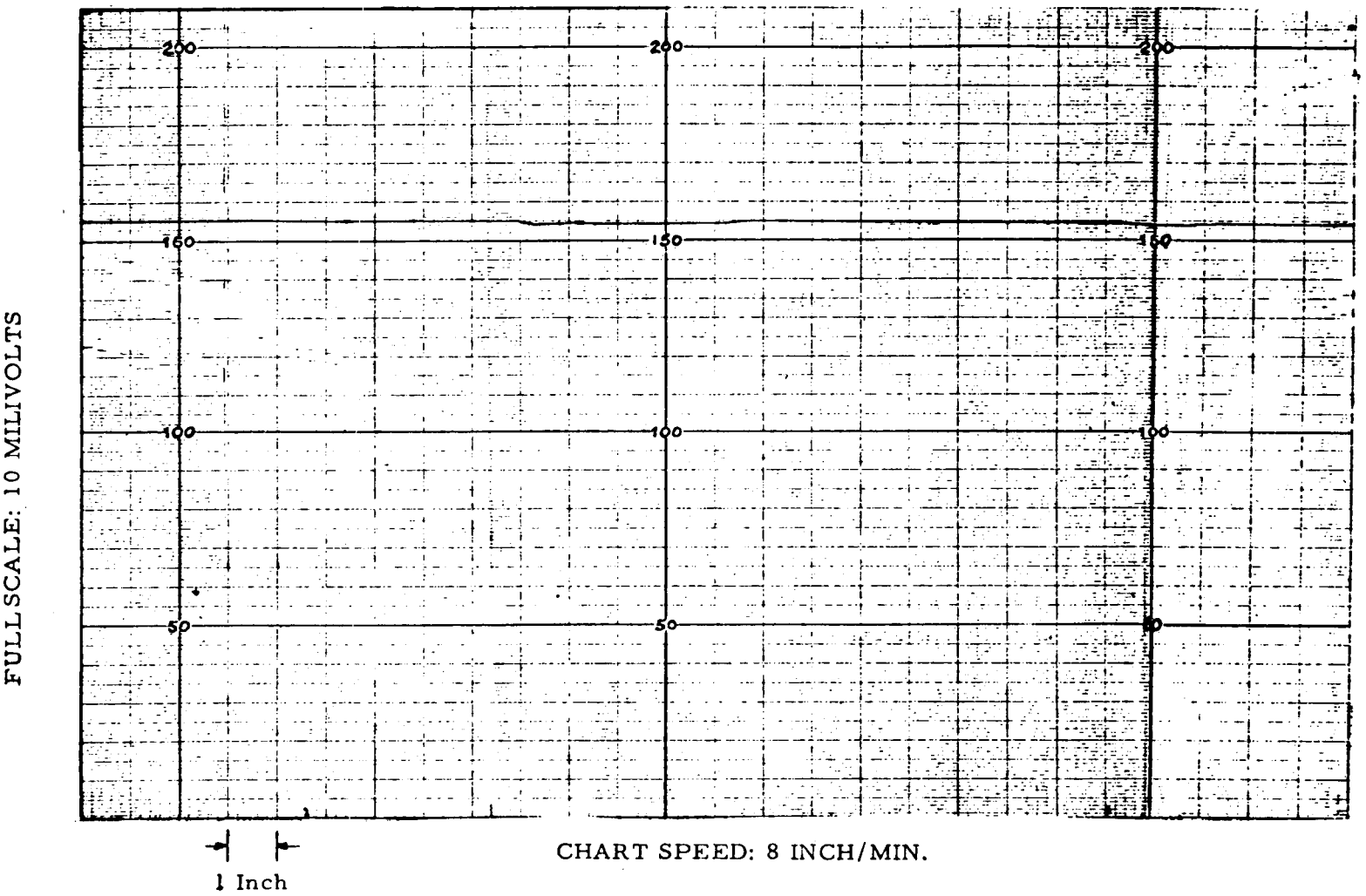

Figure 1 SOLAR FURNACE FLUX STABILITY TEST

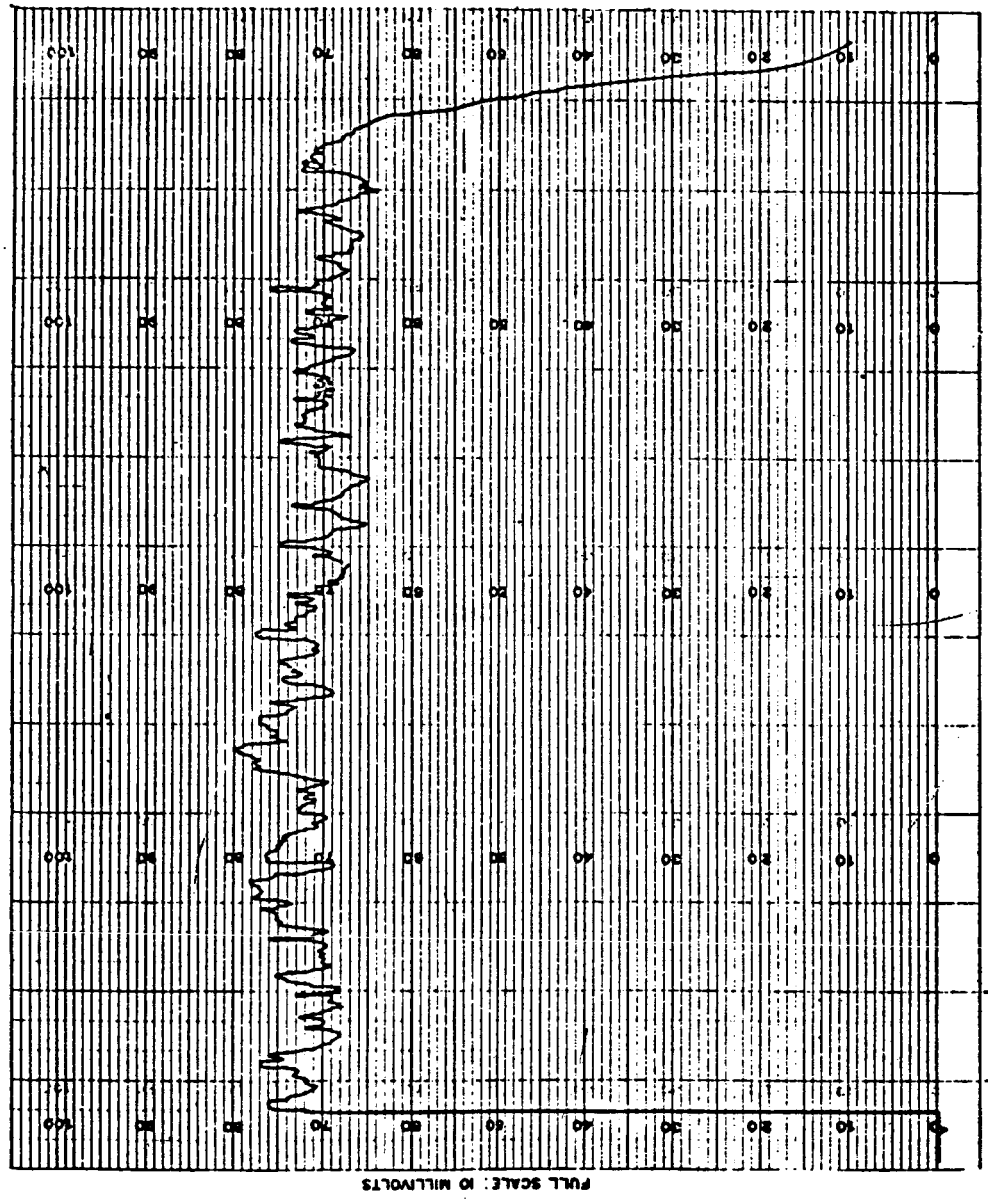

Figure 2 ARC IMAGE FURNACE FLUX STABILITY TEST

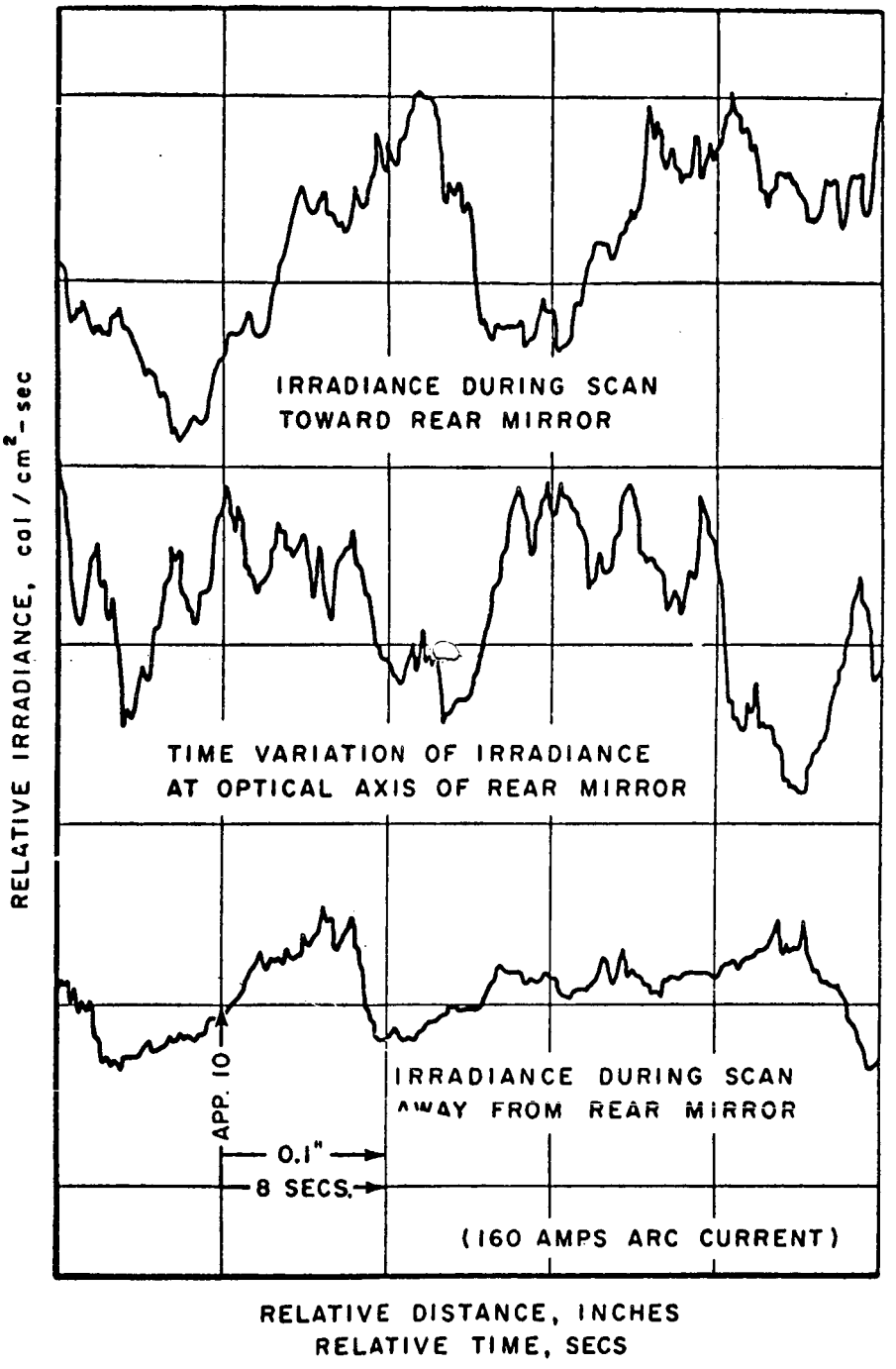

Figure 3 ARC IMAGE FURNACE FLUX VARIATION

Figure 4

REINFORCING MIRROR AROUND ANODE

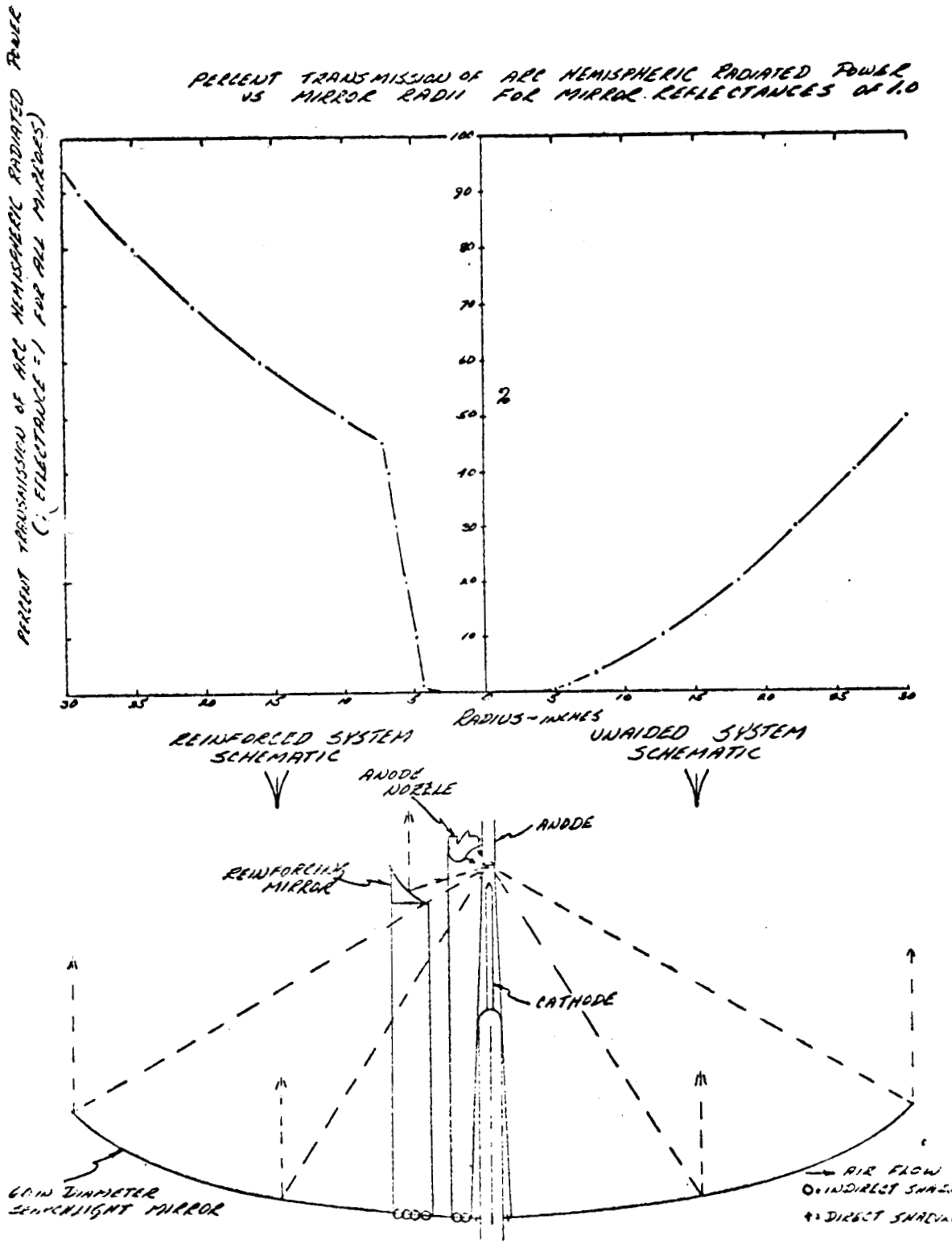

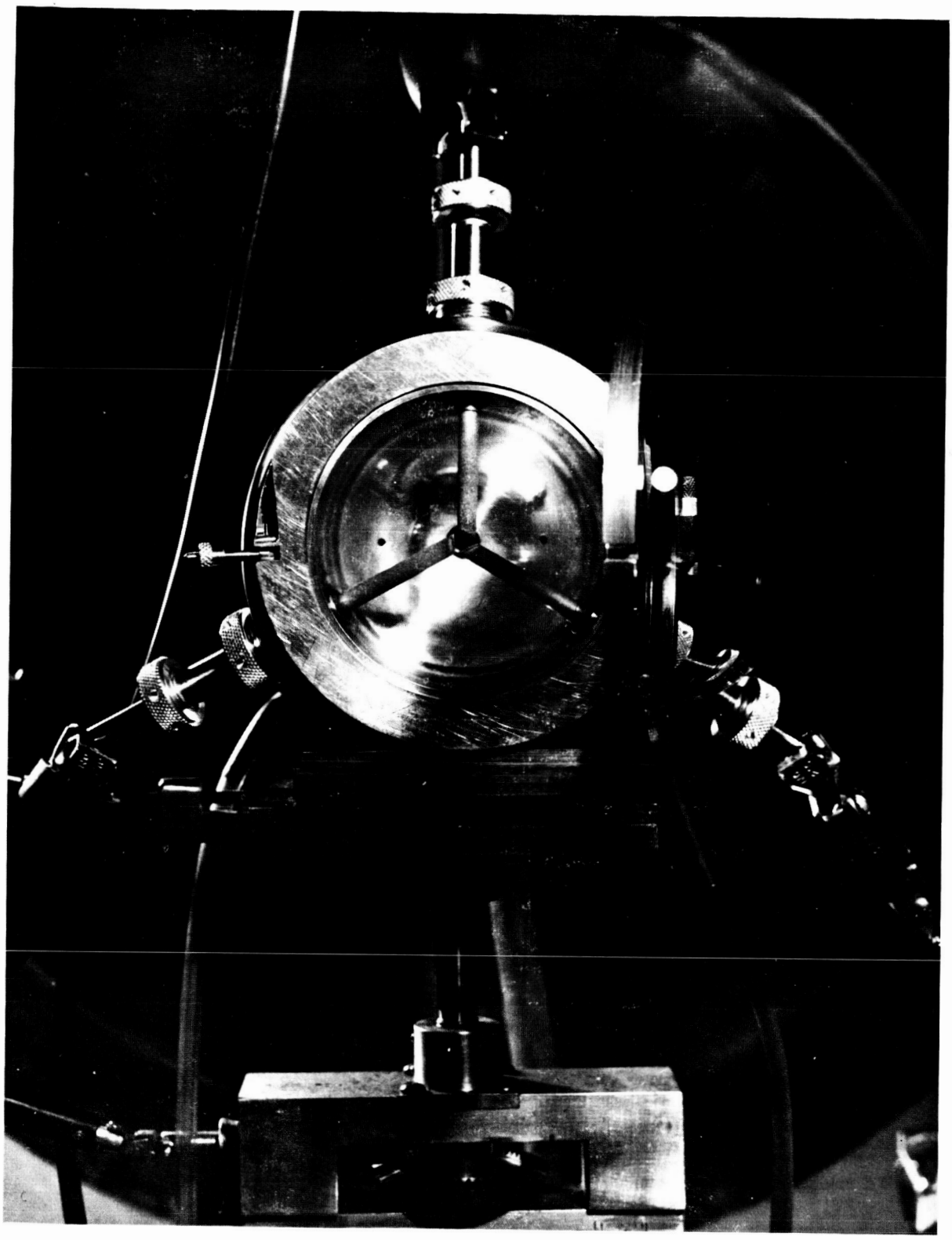

FIGURE 5 CARBON VAPOR LAMP

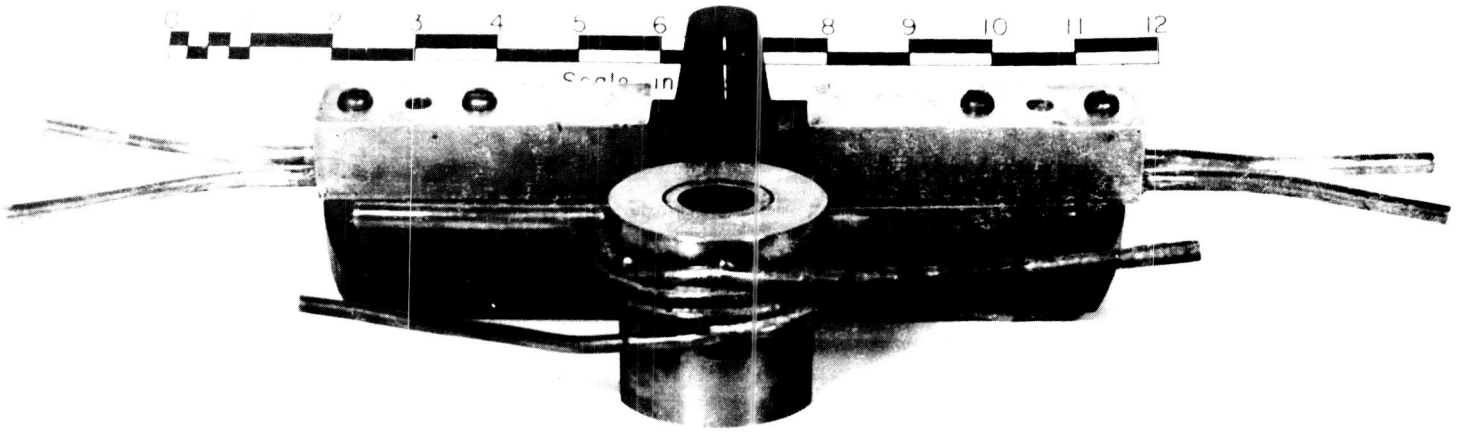

FIGURE 6 CONICAL CARBON RESISTOR

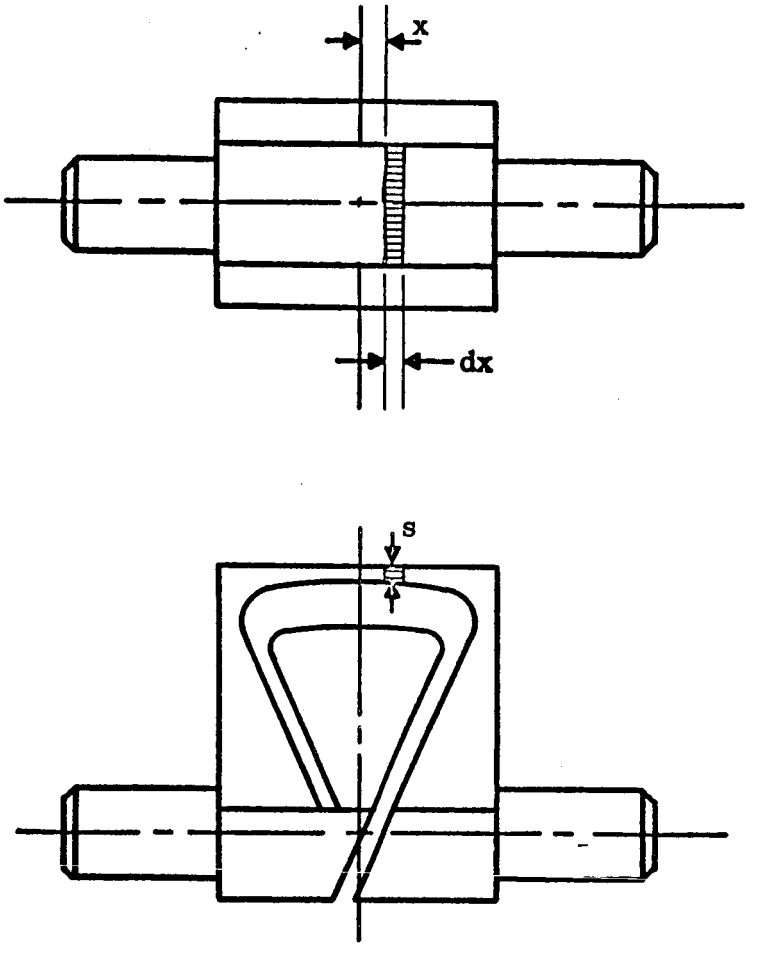

Figure 7. CARBON RADIATION SOURCE-ELEMENT

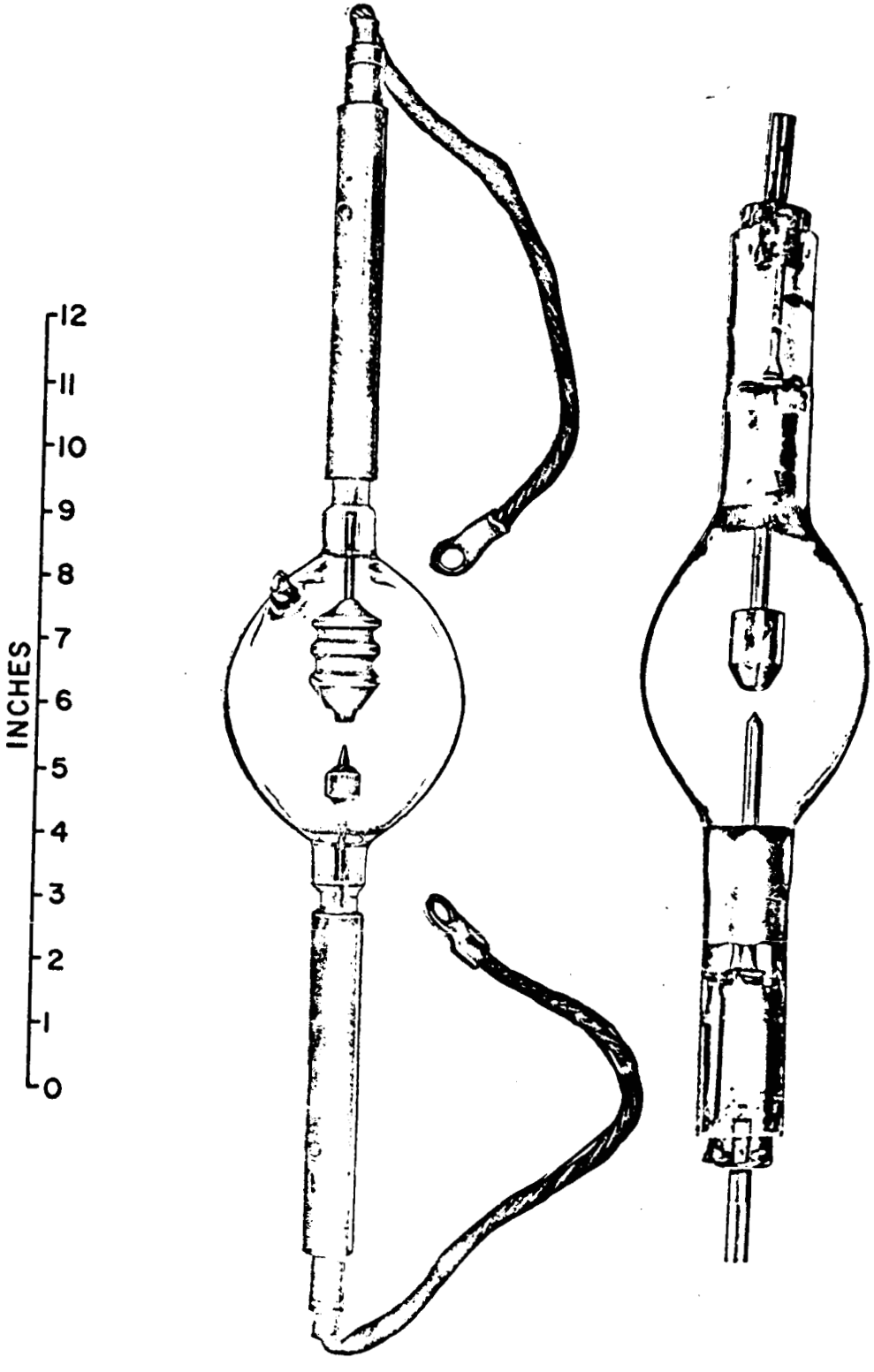

Figure 8. HIGH PRESSURE COMPACT ARCS

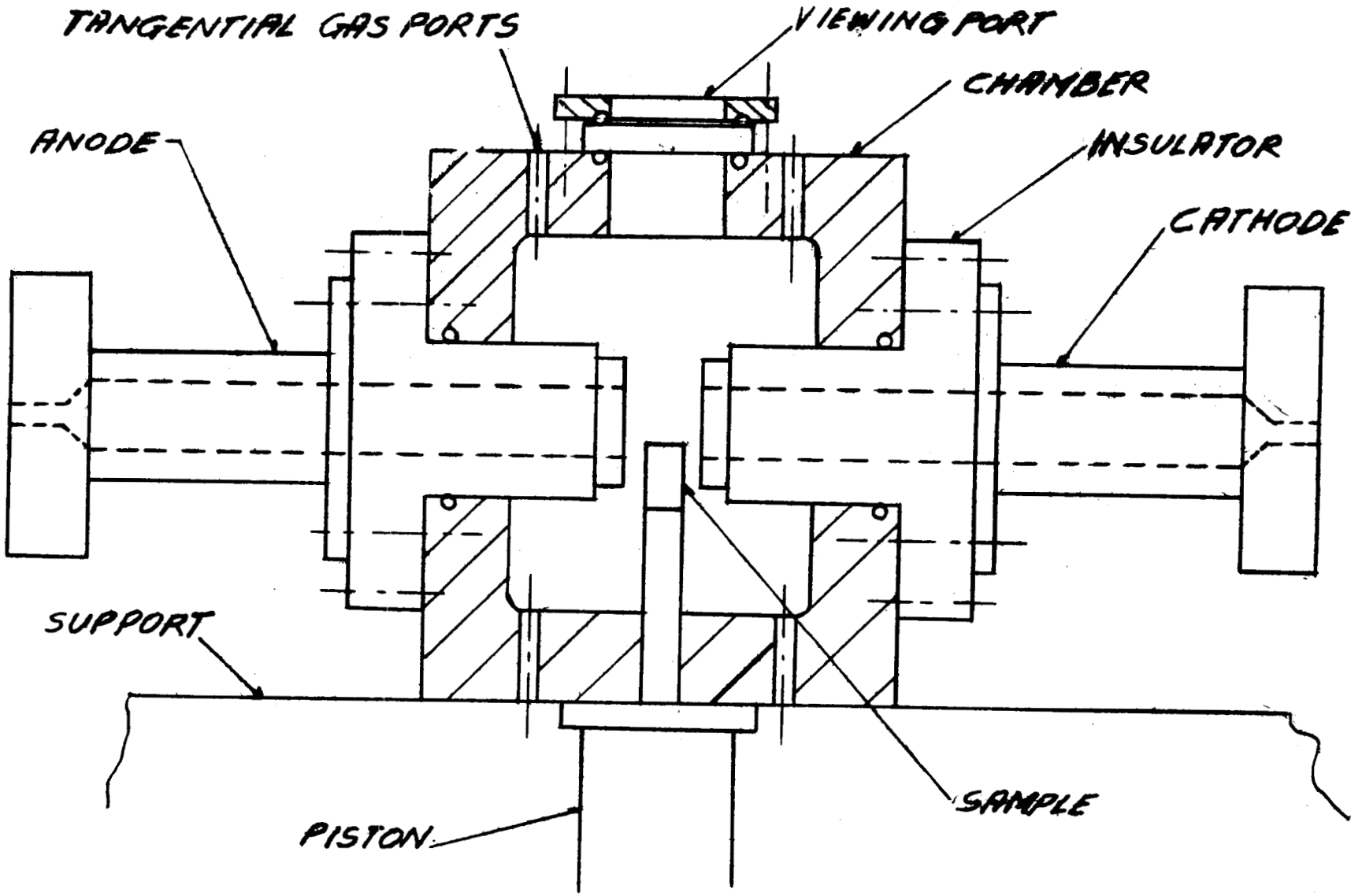

CROSS SECTION OF CONSTRICTED ARC

RADIATION SOURCE

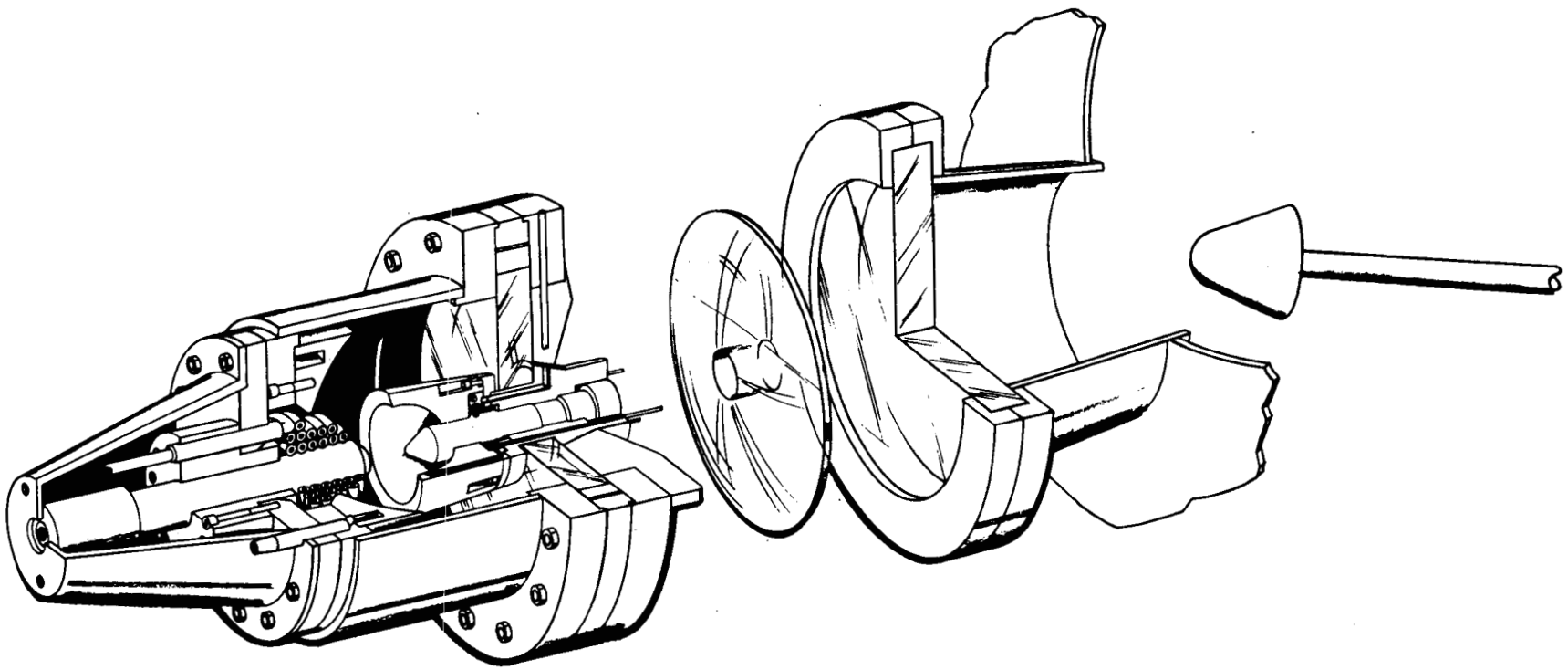

FIGURE 10

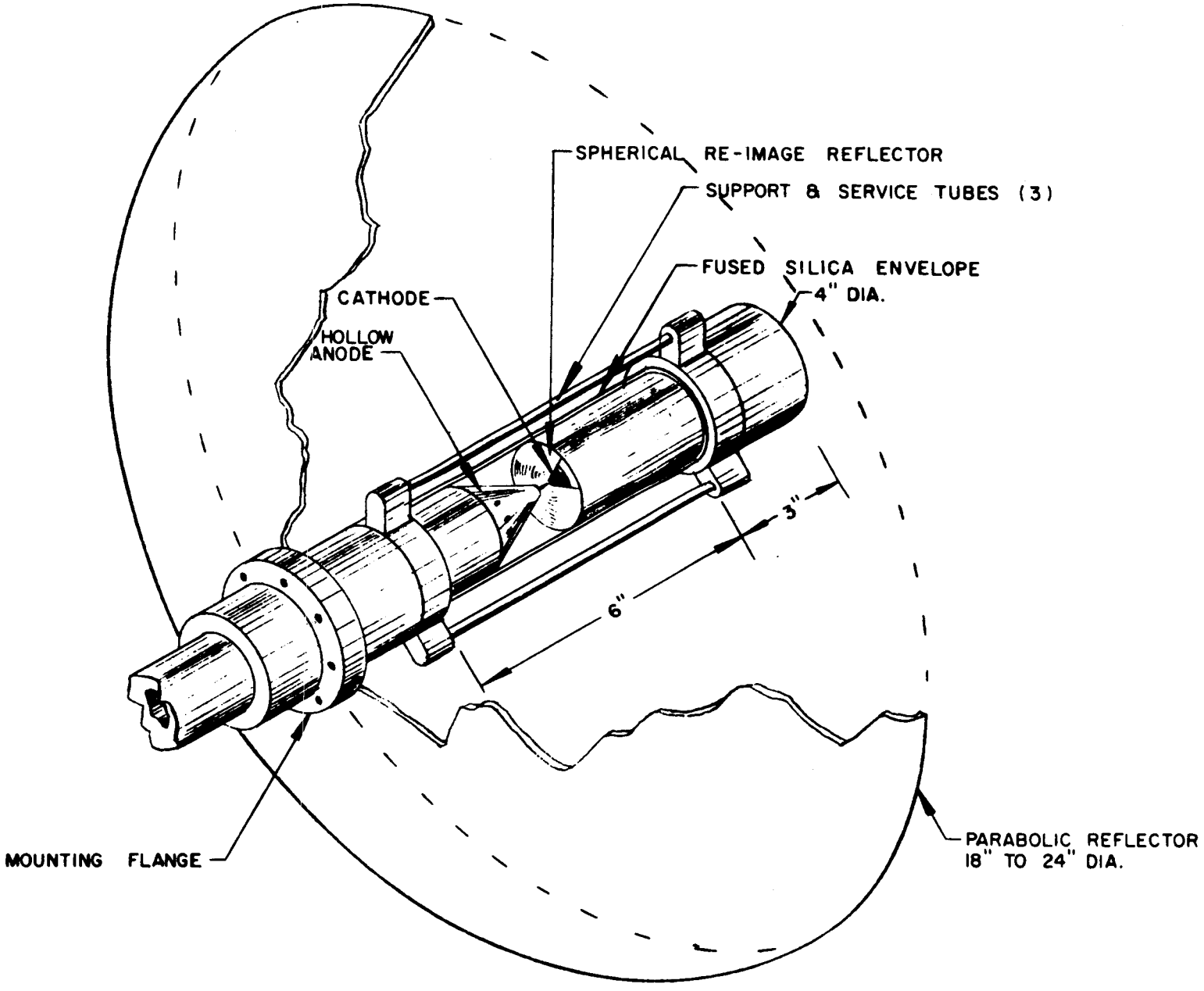

Figure 11 VORTEX STABILIZED RADIATION SOURCE

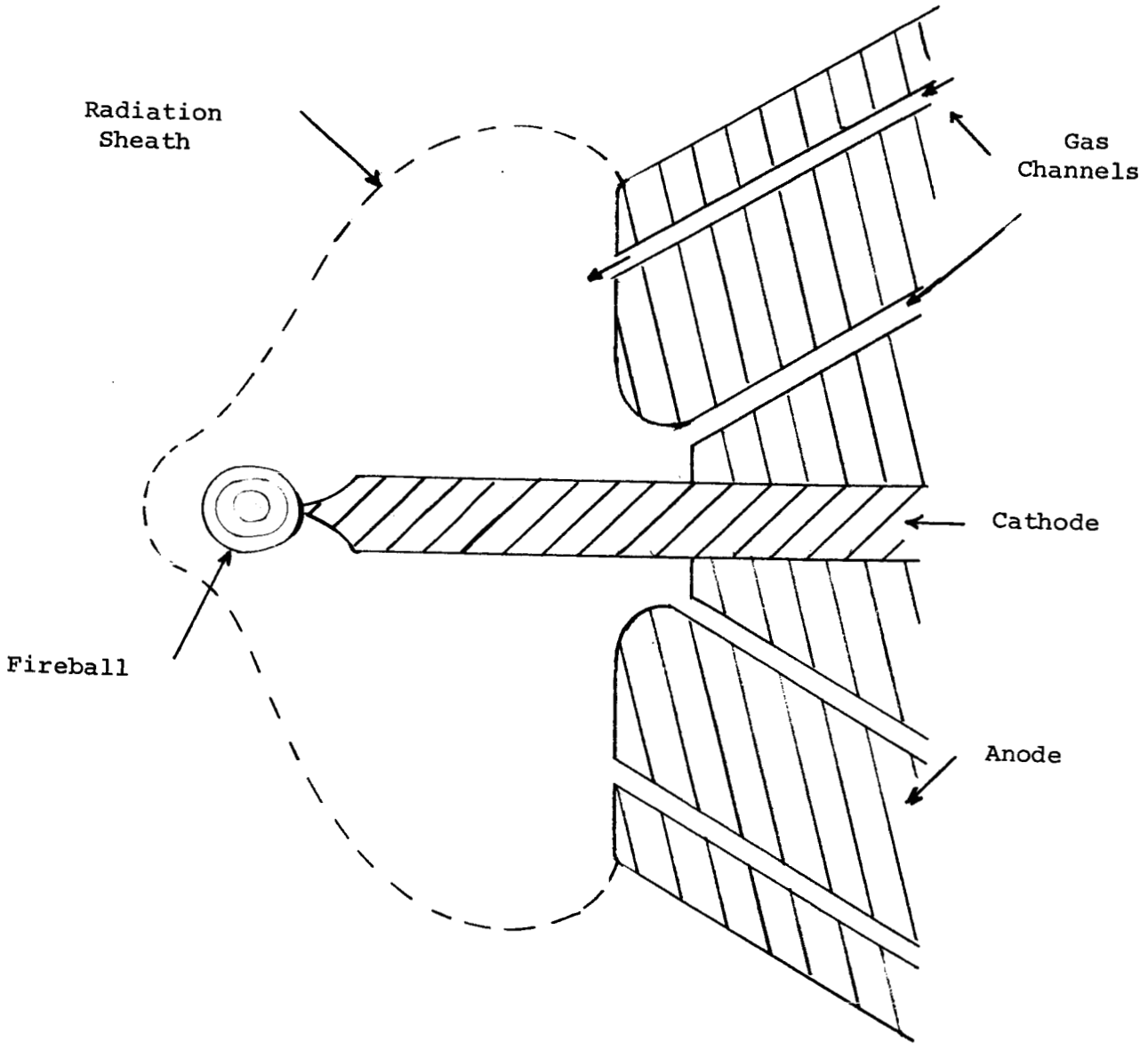

FIGURE 12 VITRO ARC SKETCH

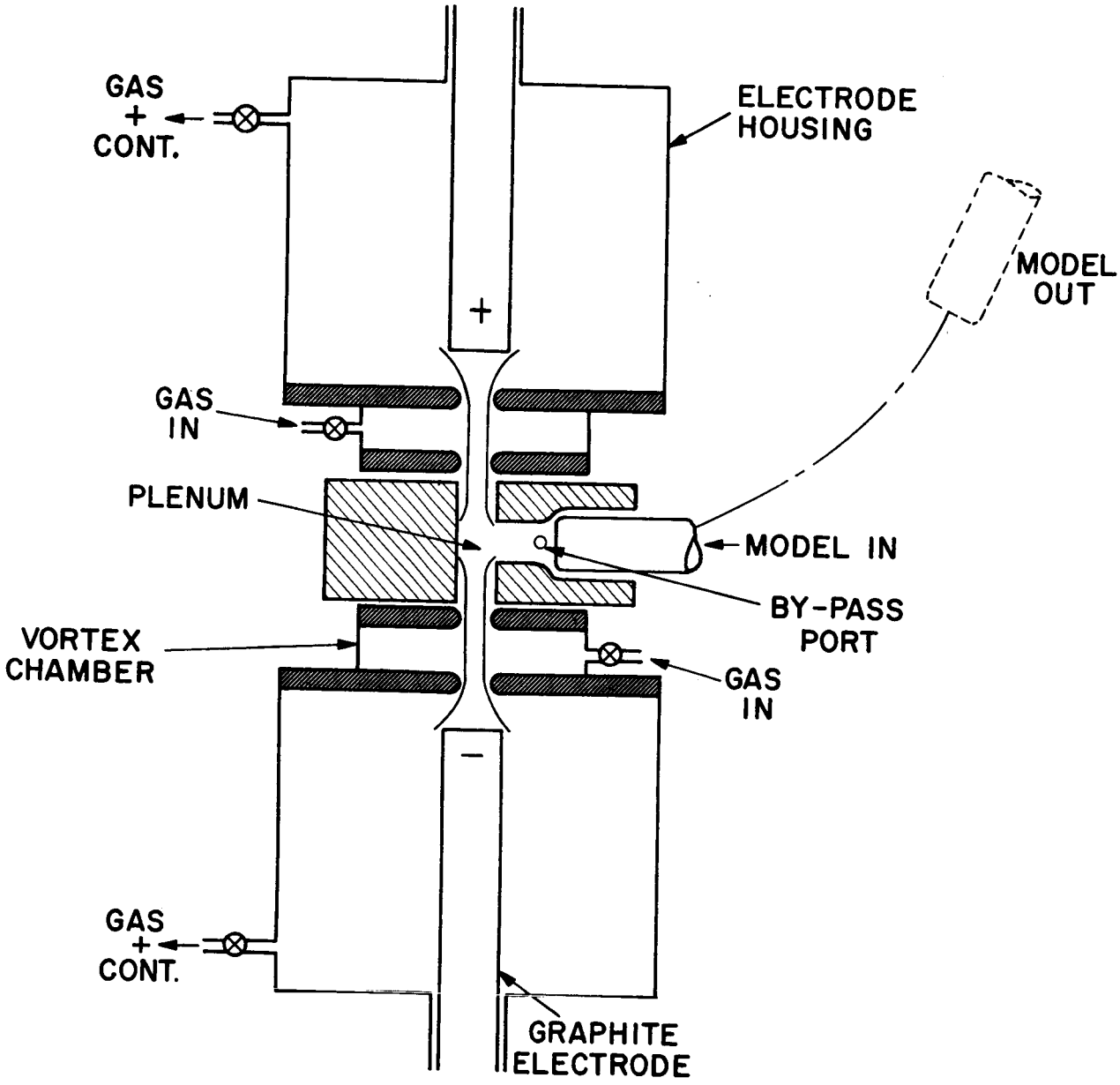

Figure 13 SCHEMATIC OF MODIFIED TANDEM GERDIEN COMBINED RADIATIVE AND CONVECTIVE HEATING ARC SOURCE

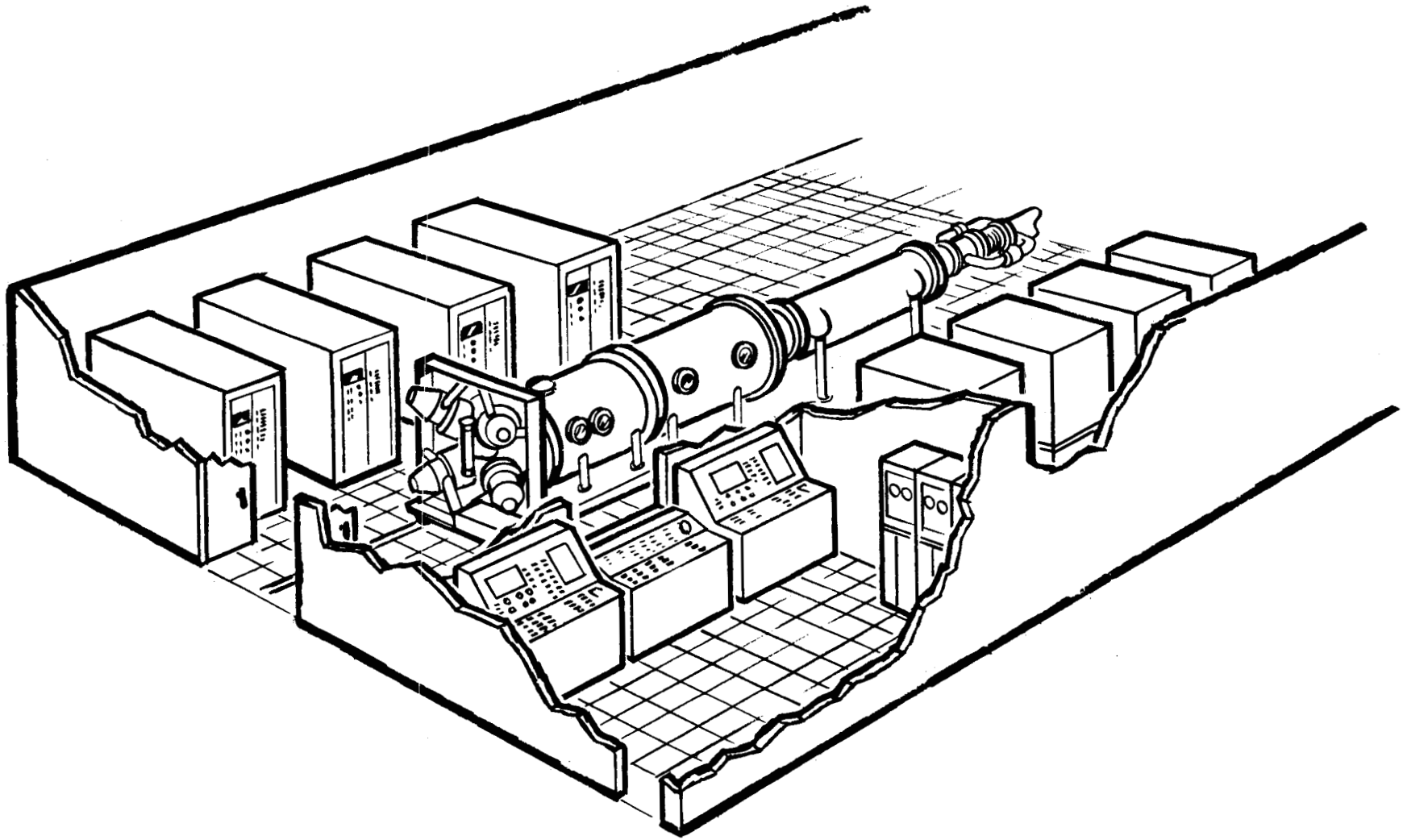

FIGURE 14 ROVERS FACILITY

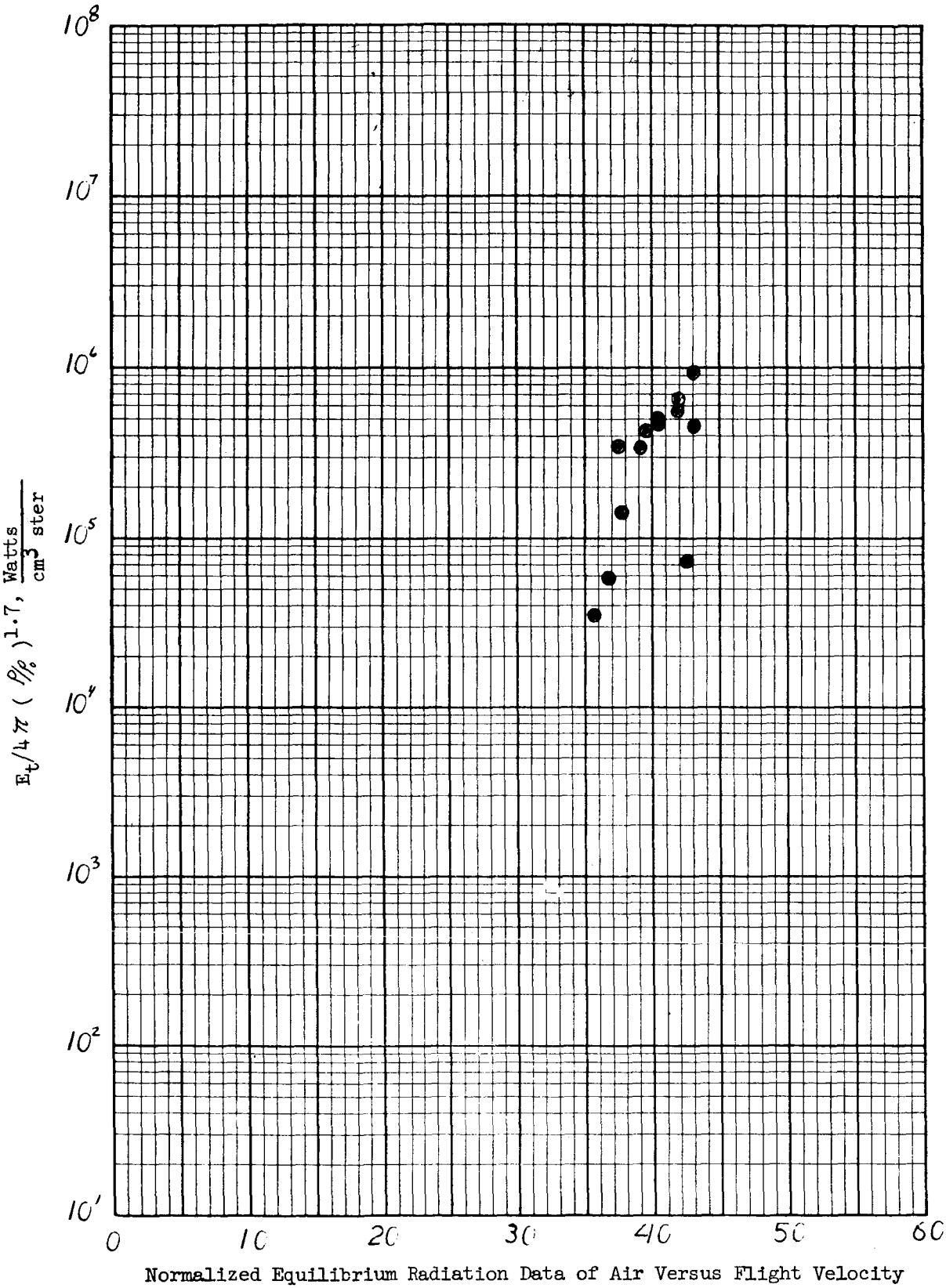
10^8
10^7
10^6
10^5
10^4
10^3
10^2
10^1
$E_t/4\pi\,(\rho/\rho_\infty)^{1.7}$, $\frac{\text{Watts}}{\text{cm}^3\ \text{ster}}$
0
10
20
30
40
50
60
Normalized Equilibrium Radiation Data of Air Versus Flight Velocity
Flight Velocity, V_∞, ft/sec x 10^{-3}

Figure 15.

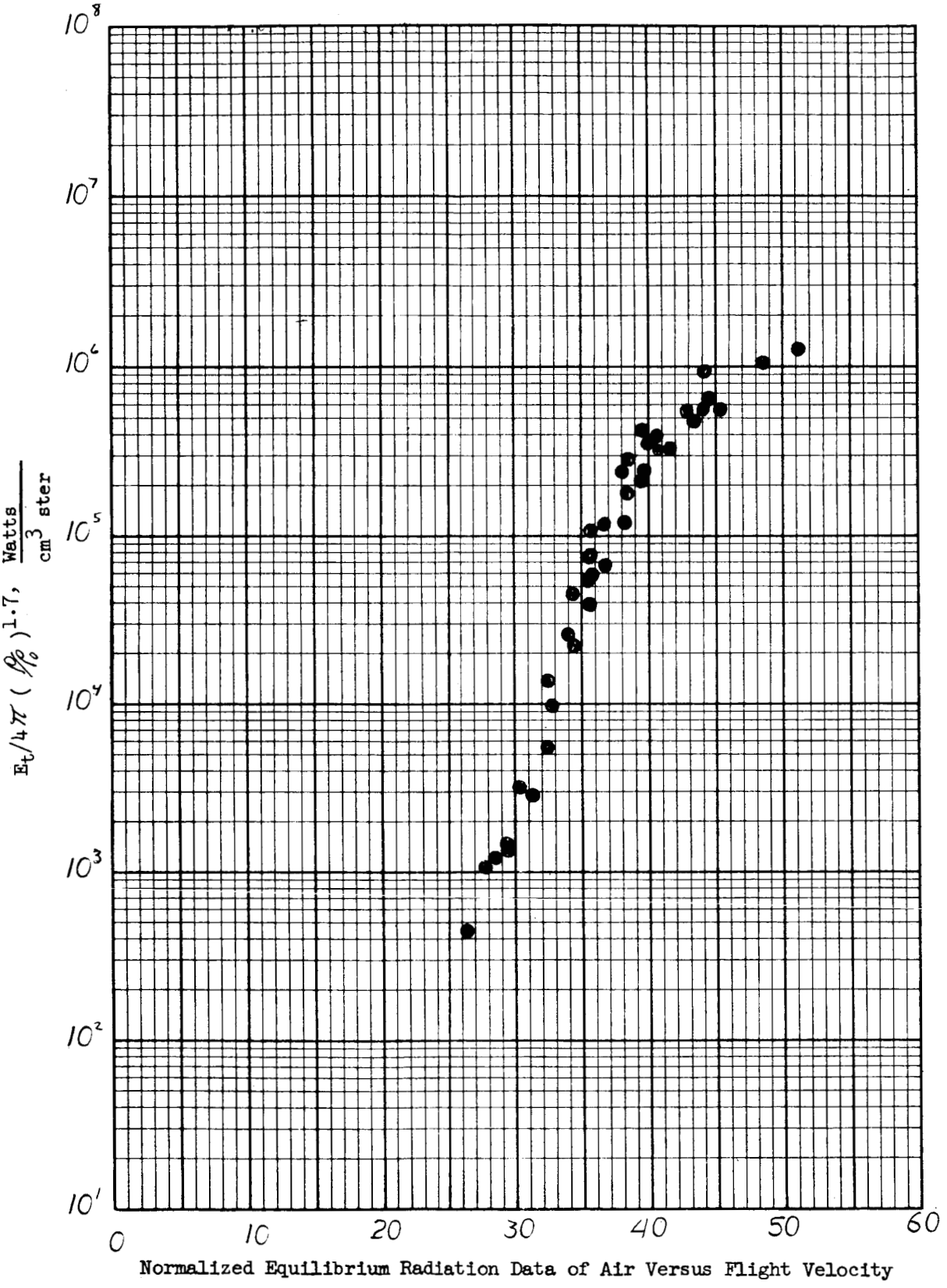
10^8
10^7
10^6
10^5
10^4
10^3
10^2
10^1
$E_t/4\pi\,(\rho_\infty)^{1.7}$, $\frac{\text{Watts}}{\text{cm}^3\,\text{ster}}$
0
10
20
30
40
50
60
Normalized Equilibrium Radiation Data of Air Versus Flight Velocity
Flight Velocity, V_∞, ft/sec x 10^{-3}

Figure 16

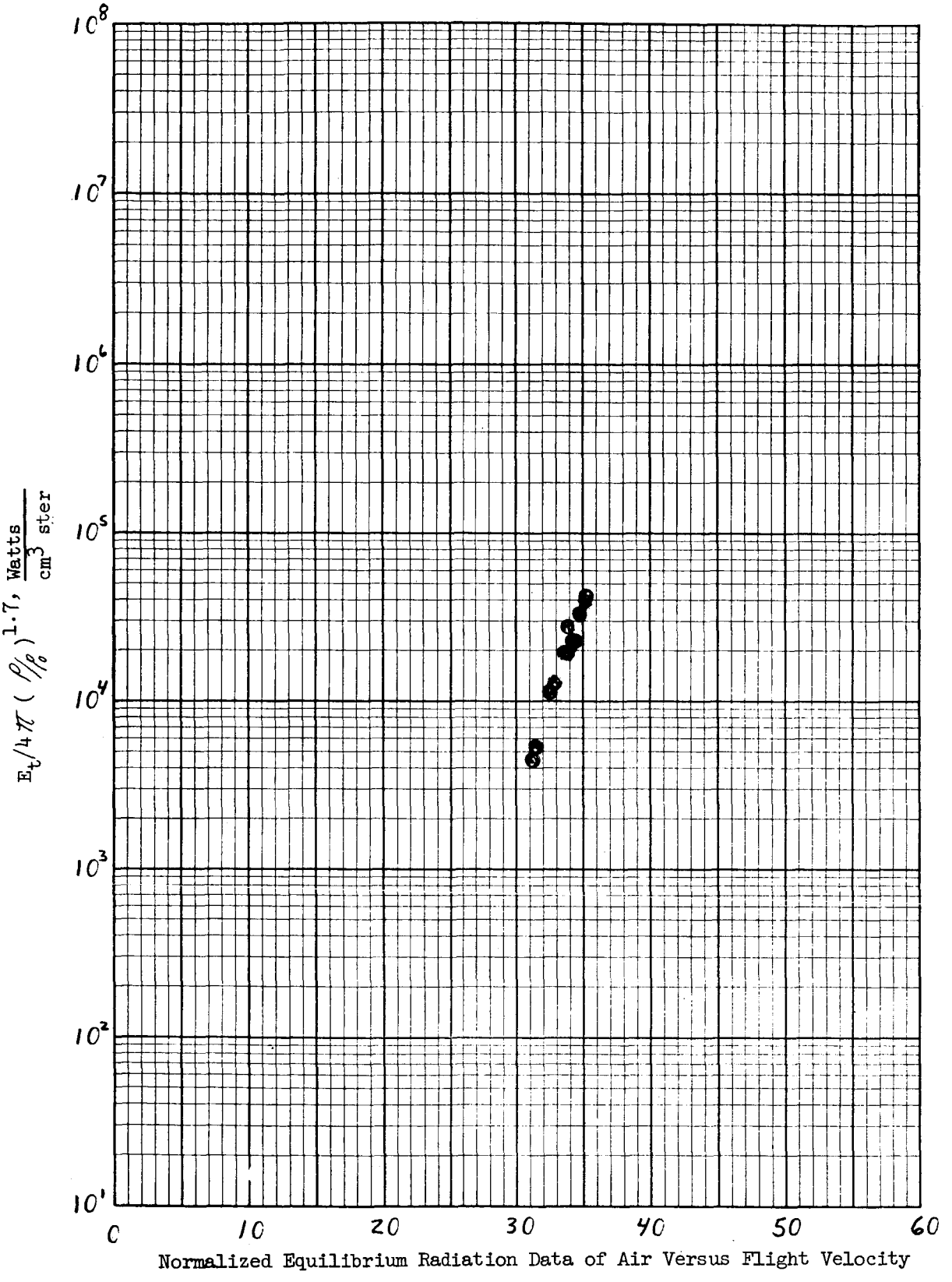

Figure 17. Flight Velocity, V_∞, ft/sec x 10^{-3}

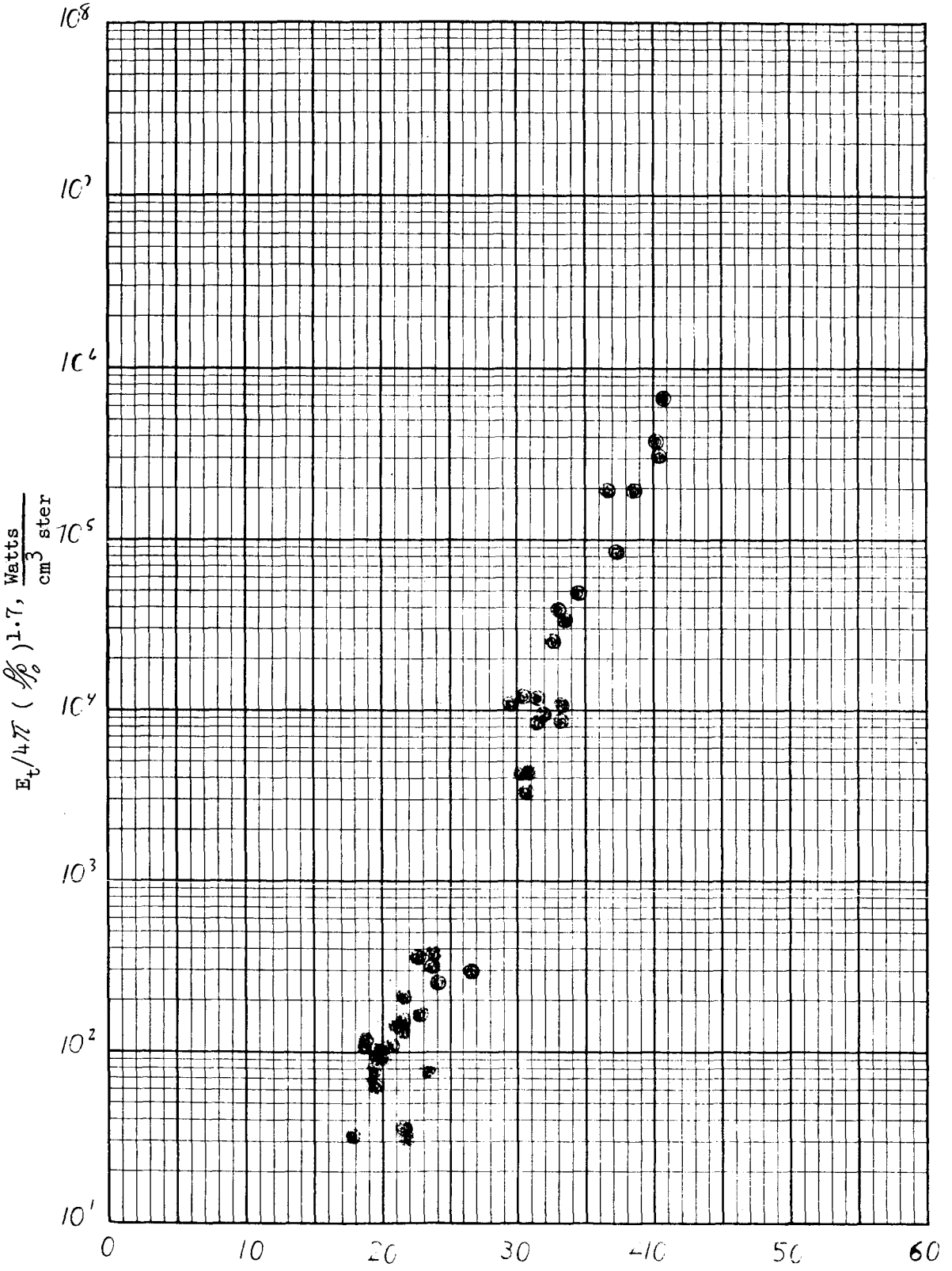

Normalized Equilibrium Radiation Data of Air Versus Flight Velocity

Figure 18.

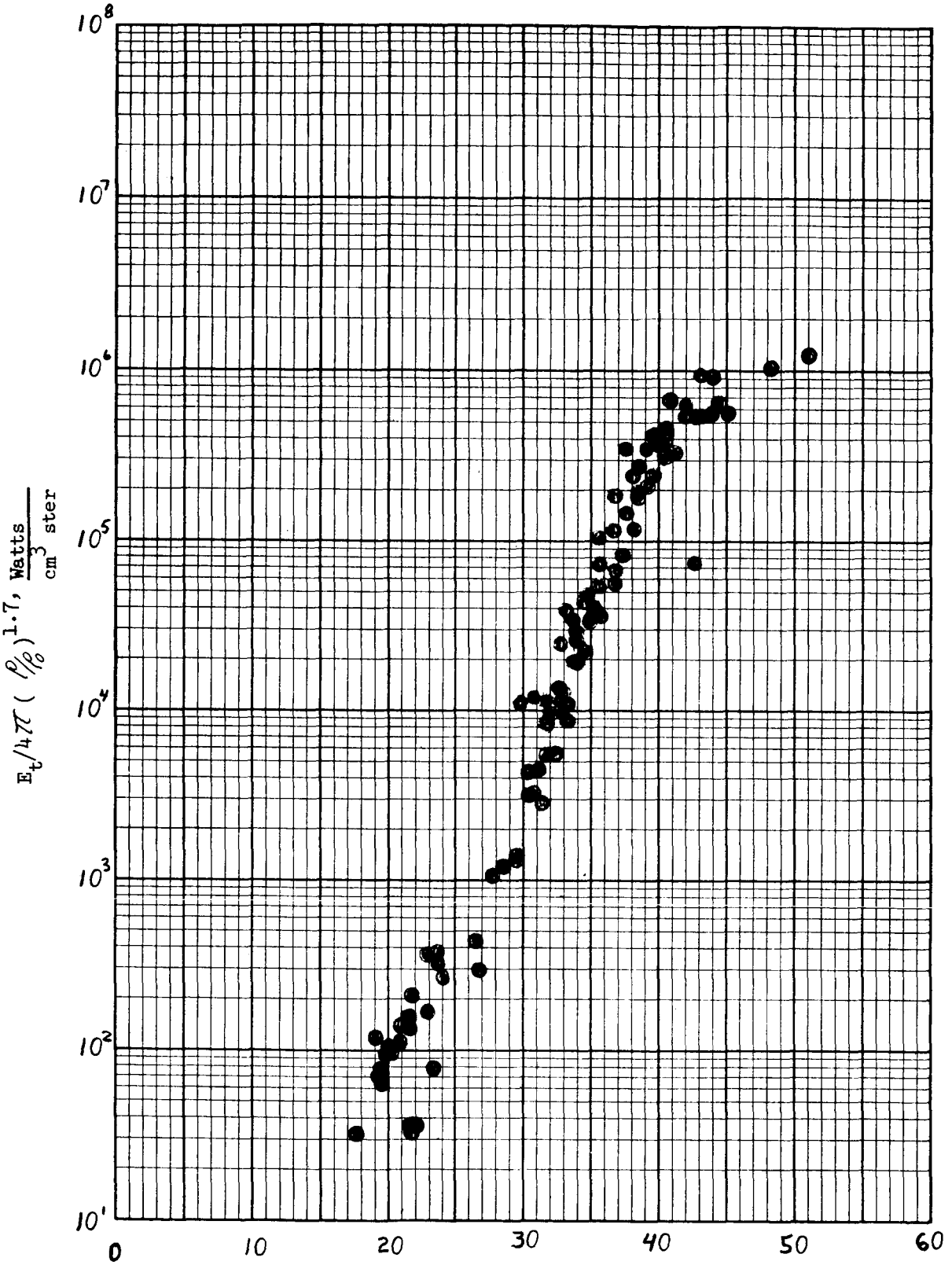
10^8
10^7
10^6
10^5
10^4
10^3
10^2
10^1
$E_t/4\pi\left(\frac{\rho}{\rho_0}\right)^{1.7}$, $\frac{\text{Watts}}{\text{cm}^3\ \text{ster}}$
0
10
20
30
40
50
60
Normalized Equilibrium Radiation Data of Air Versus Flight Velocity
Flight Velocity, V_∞, ft/sec x 10^{-3}

Figure 19.

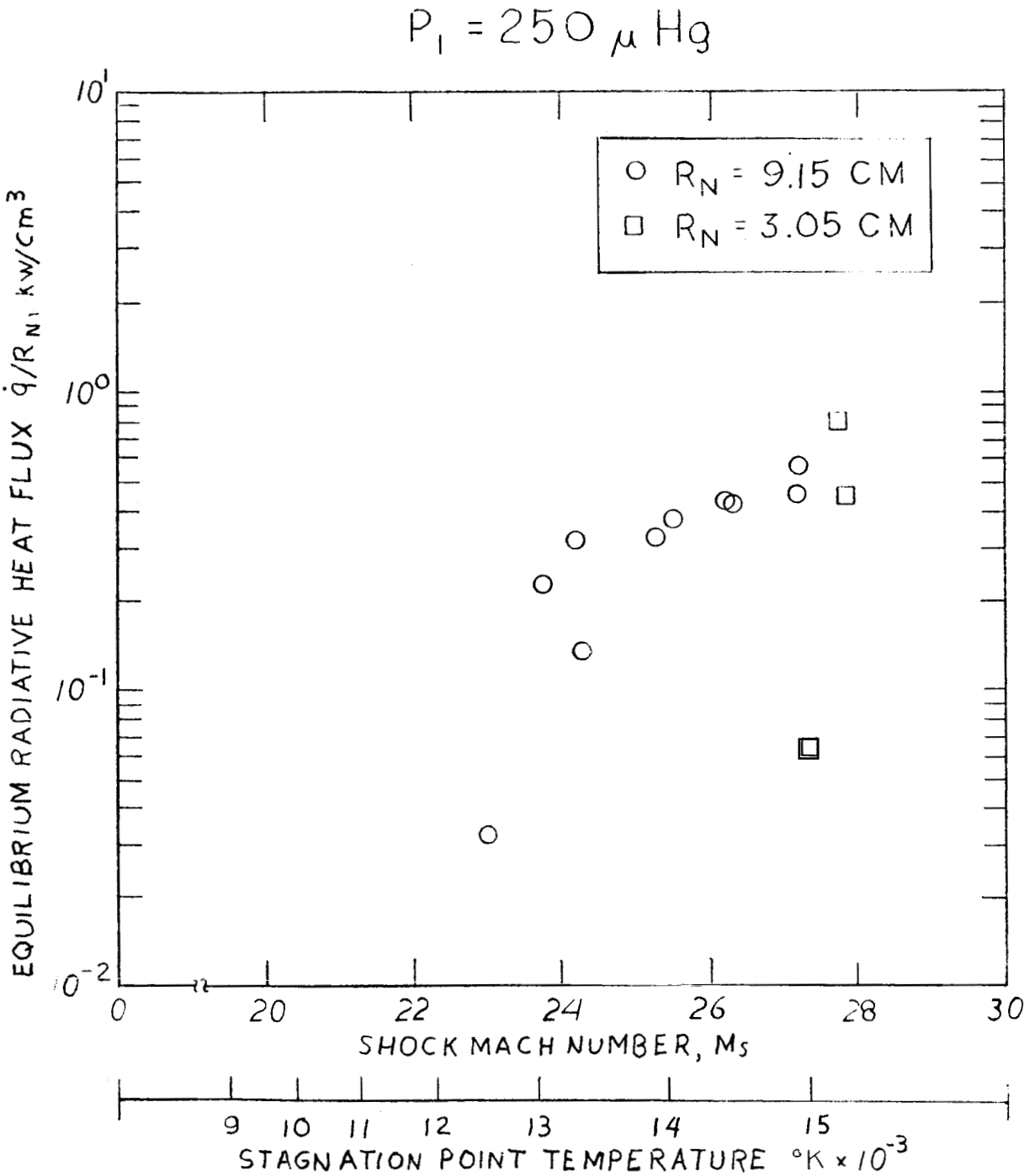

Figure 20. Flagg's Data[24]

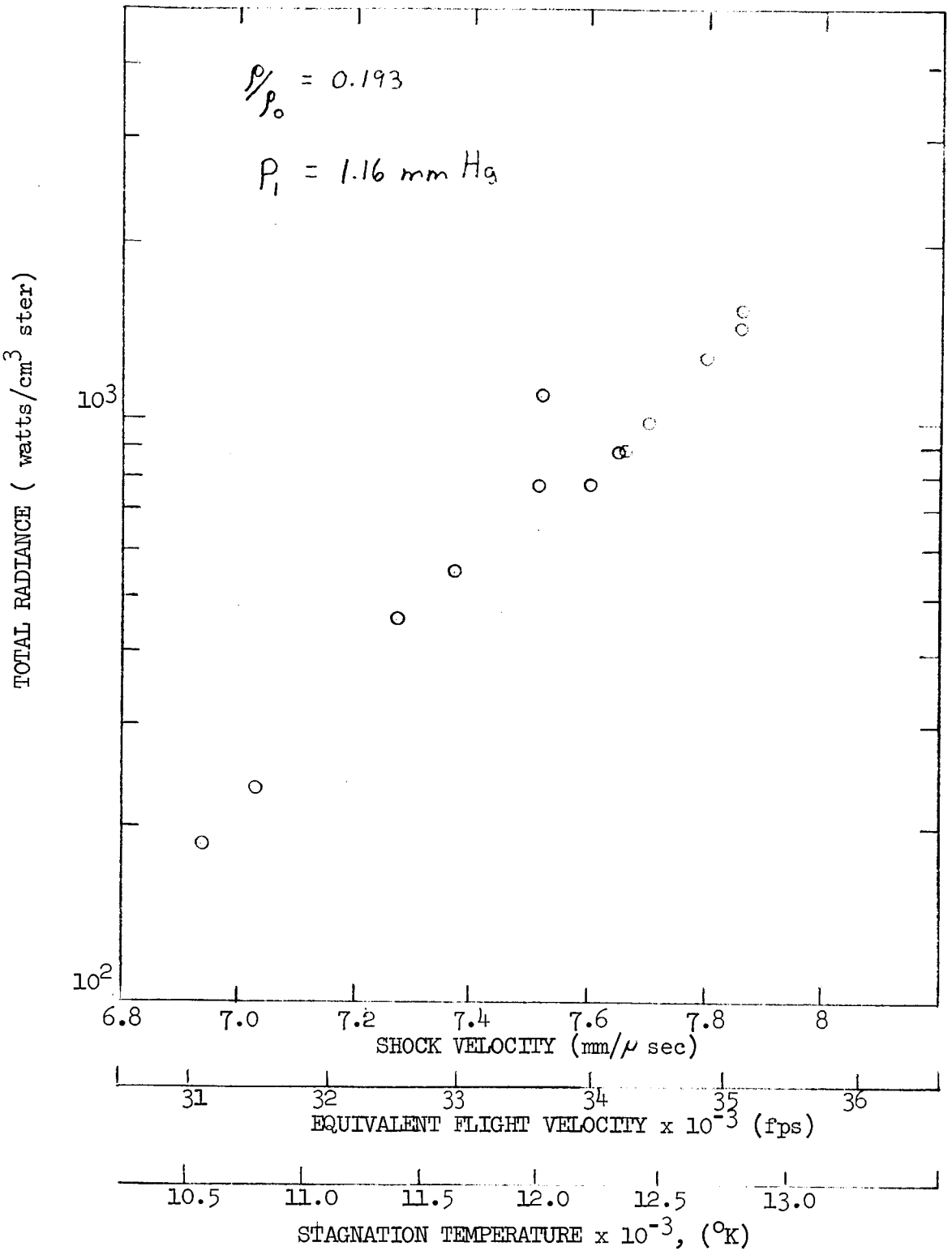

Figure 21. Hoshizaki's Data[26]